Numerical Solution of the Six-Equation Two-Phase Single Velocity Model with Finite Relaxation

Sigbjørn Løland Bore
Applied Physics, NTNU

December 19, 2014

Abstract

In this report we investigate a recently published article [6] by M. Pelanti & K.-M. Shyue on numerical simulation of two phase flow and generalize the simulation to finite relaxation. We do this by a thorough review of the theory needed to understand and simulate the model. By direct implementation of these ideas we simulate the hyperbolic part of the model using Lax–Friedrichs, HLLC– and a Roe–solver and the relaxation by the ASY–method. Our simulations not only replicates the findings in [6], they also led to finding a flaw in one of the temperature graphs. Implementation of the ASY–method for this model proved problematic due to divergences, however with a small modification of the method, these were eventually removed.

Preface

This report is a result of the pre–masters project in the final year of the masters program Applied Physics at NTNU. The work has been carried out as a collaboration between the physics faculty at NTNU and SINTEF Materials and Chemistry.

Before starting this project I was largely unfamiliar with the topic of two–phase flow. I contacted Tore Flåtten at SINTEF Materials and Chemistry and discussed the different opportunities for a project within this field. Tore being on the forefront of numerical simulation of two phase flow and me wanting to to acquire skills in computational fluid mechanics quickly agreed to do a numerical project. We chose to focus on a recently published paper by a fellow collaborator Marica Pelanti. In this paper, sophisticated numerical techniques were used for simulating Cavitating flow. We decided on the ambitious goal of replicating key results of this paper and generalizing them to finite relaxation by numerical implementation.

Working on this project has allowed me to learn a lot about numerical simulation of two phase flow. I'm also very happy with how this project has led me into the fascinating field of hyperbolic conservation laws and to understand how important having an understanding of the mathematics is for numerical study. The end result is a project that covers a wide range of topics. Our study replicates the result of [6] and found flaws in some graphs presented. The implementation of the ASY–method was problematic due to divergences. This was overcome by a small change of the method. Most important of all, this project gives a solid foundation of knowledge on which to build the master thesis.

The report is organized into multiple sections. We start out by a short introduction of two–phase flow and the model we want to simulate. We then introduce the fractional step method to motivate a separate and detailed treatment of the homogeneous part and the relaxation part. Here we present both the theory and how to numerically deal with these parts. Further we describe our numerical implementation, followed by numerical experiments done with the different techniques. Finally we end by summarizing and evaluating the future prospects of this work.

I would like thank my supervisor Dr. Tore Flåtten at Materials and Chemistry for always having and an open door and for sharing his time and insight generously with me. My thanks also goes my supervisor at the Department of Physics, Jon Andreas Støvneng for agreeing to supervise my external project without any hesitation. I would also like to thank my friend Gaute Linga at SINTEF energy for fruitful discussions and for sharing his interesting opinions on two–phase flow.

Contents

1 Introduction

In recent years a lot of attention has been put into modeling multi–phase flows – flows where multiple phases (e.g. liquid and gas) coexist and interact. These are phenomena which not only are abundant in nature, but of great industrial importance. One example we will focus on in this report is the forming of bubbles inside a liquid due to low local pressure. This process is called cavitation (illustrated in Figure 1.1) and can cause extensive damage on pipes, valves and turbines when these bubbles burst. Successful

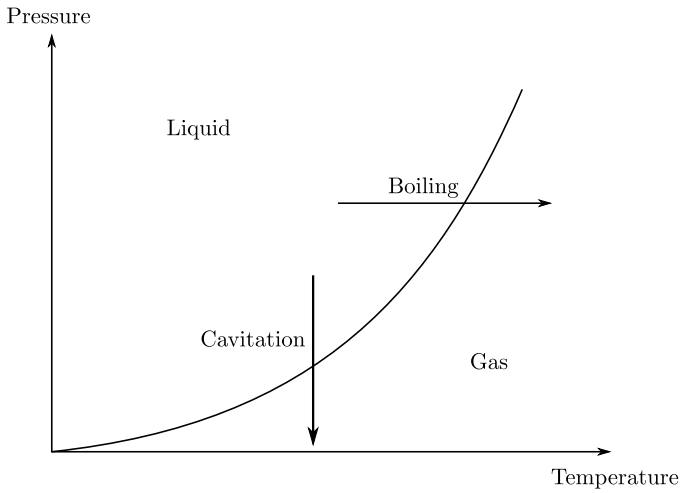

Figure 1.1: The boling curve for pressure and temperature.

modeling of multi-phase flow can yield information about how we should design the equipment in order to avoid cavitation, thereby prolonging the lifetime. From a physicist point of view a goal has been to provide models that can capture both the fluid mechanicsand interaction between the different phases, yet simple enough to be of practical use. There exist no single model for two–phase flow. The choice of model will depend on the physical problem and the demanded accuracy. Many of them belong to the category of hyperbolic–relaxation equations of the form

$$\mathbf{U}_t + \mathbf{A}(\mathbf{U})\mathbf{U}_x = \frac{1}{\epsilon}\mathbf{R}(\mathbf{U}), \tag{1.1}$$

where $\mathbf{U}$ is the quantity of interest, $\mathbf{A}(\mathbf{U})$ is a matrix[1] and $(1/\epsilon)\mathbf{R}(\mathbf{U})$ is a relaxation source term. Physically the first term represents the change of a quantity per time, for instance mass, momentum or energy. The second term will generally represent some flux of a quantity through the boundary of the control volume, for instance by convection. The source term is a relaxation term that seeks to equilibrate differences in temperature and pressure between the phases. Typically, relaxation is a very quick process compared to the flux, and happens at a very short time scale. The short time scale makes this term very stiff and requires special numerical treatment. This special treatment is complicated in combination with the hyperbolic part. A less costly method is to divide the (1.1) into two problems

$$\mathbf{U}_t = -\mathbf{A}(\mathbf{U})\mathbf{U}_x, \tag{1.2a}$$
$$\mathbf{U}_t = \mathbf{R}(\mathbf{U}) \tag{1.2b}$$

solving problem (1.2a) first and then problem (1.2b). This method is called the fractional step method, and we will present in detail later. The purpose of presenting it is to show that we can separate our problem into two parts, motivating a separate treatment of the different terms. Therefore what we need is numerical methods for dealing with hyperbolic systems and relaxation systems. We will focus on one model belonging this group, the six–equation single–velocity model of Saurel–Petitpas–Berry [8]. In this model we consider a fluid made up of two different phases $k = \{1, 2\}$. Each fluid element contains volume fraction α_k of both phases, and each phase has separate pressure, density and temperature. The

[1] In order for the system to be hyperbolic, *all* eigenvalues of $A(\mathbf{U})$ have to be real. If some of the eigenvalues are degenerate, but the eigenvectors linearly independent the system is weakly hyperbolic.

model, with volume transfer, may be transcribed as

$$\partial_t \alpha_1 + \mathbf{u} \cdot \boldsymbol{\nabla} \alpha_1 = \mu \left(p_1 - p_2 \right) \tag{1.3a}$$
$$\partial_t (\alpha_1 \rho_1) + \boldsymbol{\nabla} \cdot (\alpha_1 \rho_1 \mathbf{u}) = 0 \tag{1.3b}$$
$$\partial_t (\alpha_2 \rho_2) + \boldsymbol{\nabla} \cdot (\alpha_2 \rho_2 \mathbf{u}) = 0 \tag{1.3c}$$
$$\partial_t (\rho \mathbf{u}) + \boldsymbol{\nabla} \cdot (\rho \mathbf{u} \otimes \mathbf{u}) + \boldsymbol{\nabla} \left(\alpha_1 p_1 + \alpha_2 p_2 \right) = 0 \tag{1.3d}$$
$$\partial_t \left(\alpha_1 E_1 \right) + \boldsymbol{\nabla} \cdot (\alpha_1 E_1 \mathbf{u} + \alpha_1 p_1 \mathbf{u}) + \Sigma(q, \boldsymbol{\nabla} q) = -\mu p_I (p_1 - p_2) \tag{1.3e}$$
$$\partial_t \left(\alpha_2 E_2 \right) + \boldsymbol{\nabla} \cdot (\alpha_2 E_2 \mathbf{u} + \alpha_2 p_2 \mathbf{u}) - \Sigma(q, \boldsymbol{\nabla} q) = \mu p_I (p_1 - p_2) \tag{1.3f}$$

where α_k is the fraction of volume containing phase k, ρ_k is the density of phase–k, $\rho = \alpha_1 \rho_1 + \alpha_2 \rho_2$, $\mathbf{u}$ is the common velocity of both phases (single velocity model), E_k is the total energy of each phase and

$$\Sigma(\mathbf{U}, \boldsymbol{\nabla} \mathbf{U}) = -\mathbf{u} \cdot \left(Y_2 \boldsymbol{\nabla} (\alpha_1 p_1) - Y_1 \boldsymbol{\nabla} \left(\alpha_2 p_2 \right) \right). \tag{1.4}$$

Ignoring the relaxation terms and the volume fractions, these are essentially the Euler equations for each phase. To put this model into the general context of hyperbolic conservation laws it is useful to consider (1.3) in the following form

$$\partial_t \mathbf{U} + \boldsymbol{\nabla} \cdot \mathbf{f}(\mathbf{U}) + \boldsymbol{\sigma}(\mathbf{U}, \boldsymbol{\nabla} \mathbf{U}) = \boldsymbol{\psi}_\mu, \tag{1.5}$$

where

$$\mathbf{f}(\mathbf{U}) = \begin{pmatrix} 0 \\ \alpha_1 \rho_1 \\ \alpha_2 \rho_2 \mathbf{u} \\ \rho \mathbf{u} \otimes \mathbf{u} + \alpha_1 p_1 + \alpha_2 p_2 \\ \alpha_1 E_1 \mathbf{u} + \alpha_1 p_1 \mathbf{u} \\ \alpha_2 E_2 \mathbf{u} + \alpha_2 p_2 \mathbf{u} \end{pmatrix}, \boldsymbol{\sigma}(\mathbf{U}) = \begin{pmatrix} \mathbf{u} \cdot \boldsymbol{\nabla} \alpha_1 \\ 0 \\ 0 \\ 0 \\ \Sigma(\mathbf{U}, \boldsymbol{\nabla} \mathbf{U}) \\ -\Sigma(\mathbf{U}, \boldsymbol{\nabla} \mathbf{U}) \end{pmatrix}, \boldsymbol{\psi}(\mathbf{U}) = \begin{pmatrix} \mu (p_1 - p_2) \\ 0 \\ 0 \\ 0 \\ -\mu p_I (p_1 - p_2) \\ \mu p_I (p_1 - p_2) \end{pmatrix}, \tag{1.6}$$

and

$$\mathbf{U} = \begin{pmatrix} \alpha_1 \\ \alpha_1 \rho_1 \\ \alpha_2 \rho_2 \\ \rho \mathbf{u} \\ \alpha_1 E_1 \\ \alpha_2 E_2 \end{pmatrix}, \tag{1.7}$$

where $\mathbf{f}$ contains conservative flux terms and $\boldsymbol{\sigma}$ contains spatial derivatives of non–conservative form. Finally, $\boldsymbol{\psi}$ is a mechanical relaxation term, that seeks to equalize the pressures. Special care needs to be taken in handling each term. We will start out by considering the "homogeneous system part", $\boldsymbol{\psi} = 0$.

2 Hyperbolic conservation equations

To understand the contribution of the flux–term to the overall behavior to the system and how to treat it numerically, a basic understanding of hyperbolic conservation laws is needed. We will follow to a large the degree the approach of Randall Leveque in [5]. Conservation laws are derived by considering a conserved quantity of a system, this can be total mass, momentum, energy etc. The change of a conserved quantity $\mathbf{U}$ inside a control volume is given by

$$\frac{\partial}{\partial t}\int_{\Omega}\mathbf{U}\mathrm{d}V + \int_{\partial\Omega}\mathbf{F}(\mathbf{U})\cdot\hat{\mathbf{n}}\mathrm{d}A = 0, \tag{2.1}$$

which can be interpreted as the change of $\mathbf{U}$ inside the control volume is equal to the flux of $\mathbf{U}$ through the boundary of the control volume. This form is the most general, but solving actual problems with this form is very cumbersome, as we have an integral equation and not a partial differential equation. A partial differential equation formulation is obtained by the Gauss theorem

$$\frac{\partial}{\partial t}\int_{\Omega}\mathbf{U}\mathrm{d}V + \int_{\Omega}\boldsymbol{\nabla}\mathbf{F}(\mathbf{U})\mathrm{d}V = 0, \tag{2.2}$$

and by the fundamental theorem of calculus this can be written as a partial differential equation

$$\frac{\partial\mathbf{U}}{\partial t} + \boldsymbol{\nabla}\mathbf{F}(\mathbf{U}) = 0. \tag{2.3}$$

Remark It is important to note that in obtaining this equation we have assumed that $\mathbf{U}$ is a continuous function. However, this is not always the case. For nonlinear conservation equations, discontinuous solutions can emerge from continuous initial conditions. In such situations we are forced to return to the original integral formulation.

2.1 Characteristic solutions

A key to understand conservation laws is the concept of characteristic solutions. Solutions of hyperbolic systems are constant on characteristic lines. The simplest example that illustrates this is the scalar advection law

$$u_t + (au)_x = 0, \tag{2.4}$$

where a is a constant advection speed. The solution of this equation is

$$u = u_0(x - at). \tag{2.5}$$

We see here that the solution is constant on lines of

$$x = at. \tag{2.6}$$

Figure 2.1 shows how the initial condition is advected by traveling on characteristic lines in the time and position space.

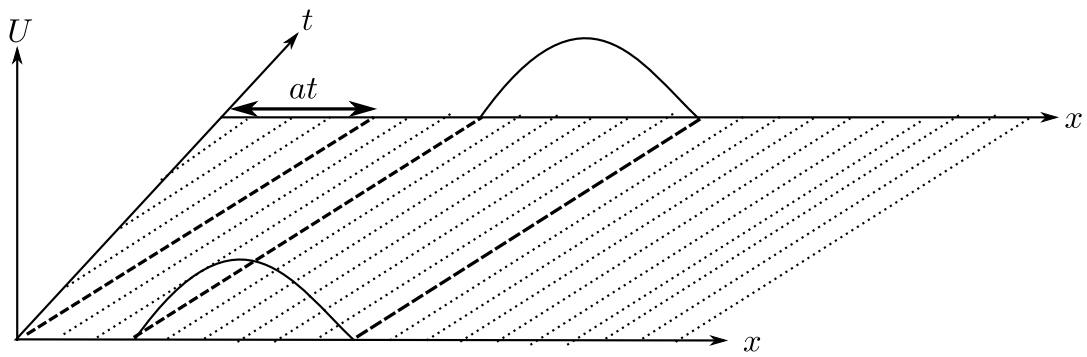

Figure 2.1: Illustration of how initial solution travels on characteristics.

To generalize this concept to systems in 1–d we start by writing (2.3) in quasilinear form[2]

$$\mathbf{U}_t + \frac{\partial \mathbf{F}(\mathbf{U})}{\partial \mathbf{U}} \mathbf{U}_x = 0 \tag{2.7}$$

$$\mathbf{U}_t + \mathbf{A}(\mathbf{U})\mathbf{U}_x = 0, \tag{2.8}$$

where $\mathbf{A}(\mathbf{U})$ now is a matrix, called the Jacobian of the system. Multiplying by the similarity matrix $\mathbf{T}^{-1}$ we diagonalize our system of equations

$$\mathbf{T}^{-1}\mathbf{U}_t + \mathbf{T}^{-1}\mathbf{A}\mathbf{U} \tag{2.9}$$

$$\mathbf{T}^{-1}\mathbf{U}_t + \mathbf{T}^{-1}\mathbf{A}\mathbf{T}\mathbf{T}^{-1}\mathbf{U} \tag{2.10}$$

$$\mathbf{V}_t + \mathbf{D}\mathbf{V}_x = 0 \tag{2.11}$$

where $\mathbf{V} = \mathbf{T}^{-1}\mathbf{U}$ and $\mathbf{D}$ is a diagonal matrix given by $\mathbf{D} \equiv \text{diag}\,(\lambda_1, \ldots, \lambda_n)$, where n is the number of components. We will limit ourself to hyperbolic systems, for which all eigenvalues are real. Componentwise (2.11) can be written as

$$\frac{\partial V_i}{\partial t} + \lambda_i \frac{\partial V_i}{\partial x} = 0. \tag{2.12}$$

For a linear conservation law ($\mathbf{A}(\mathbf{U}) = \mathbf{A}$), this corresponds to a set of independent advection equations with advection speed a replaced by the eigenvalue λ_i. The solutions of these are given by $V_i = V_{i0}(x - \lambda_i t)$. Its important to note that it is the characteristic components of $\mathbf{V}$ that are advected and not vU. $\mathbf{U}$ is only obtained through

$$\mathbf{U} = \mathbf{T}\mathbf{V}. \tag{2.13}$$

This method of finding the solution is limited to linear systems. However, the eigenstructure of the conservation equations can also elucidate how a general system behaves. For a general hyperbolic system of equations, we can interpret the eigenvalues as the speeds at which characteristic variables or information travels. In case of the Euler equation, the eigenvalues are given by a combination of the fluid speed and the speed of sound. In addition to telling us at which speeds the information travels, they also tell us the direction it travels. This is key when prescribing boundary conditions. Variables traveling to the right needs to be prescribed at the left and vice versa. Not doing so correctly can lead to ill posed problems.

2.2 Nonlinear conservation laws and shock formation

Having an understanding of how a linear systems behaves, is crucial for the understanding of a general nonlinear system. However, new phenomena will emerge when we go to the nonlinear case. The eigenstructure still holds true for a nonlinear system, however the eigenvalues will be dependent on $\mathbf{U}$. This means that how fast the characteristic variables travel will depend on local configuration. The simplest example of what can occur is the Burgers equation

$$u_t + (\frac{1}{2}u^2)_x = 0,$$

and in in quasilinear form,

$$u_t + uu_x = 0. \tag{2.14}$$

Similarly to the advection equation, the solution can be written implicitly as follows

$$u = u(x - ut), \tag{2.15}$$

where now the eigenvalue is given by u. This means that the solution is constant on lines of $x = ut$. Thus starting from initial values $u_0(x)$, solutions travel on lines $x = u_0 t$. The best way to visualize this is by drawing lines in the (x, t)–plane as in Figure 2.2. Firstly note that like for the advection equation the lines are straight, however due to the nonlinearity the slope differ dependent on the initial velocity. We see in the right graph that solutions with high initial velocity will travel faster to the right than solutions with low initial velocity. This results in the creation of a *shock* at $t = 0.3$, shown in Figure 2.2 – a discontinuity in the solution. Note that the time when this sharp discontinuity appears coincides with the time the characteristic lines start intersecting. At time $t = 1$ we see that the solution is no

[2]For a linear system $\mathbf{F}(\mathbf{U}) = \mathbf{A}\mathbf{U}$, where $\mathbf{A}$ is independent of $\mathbf{U}$.

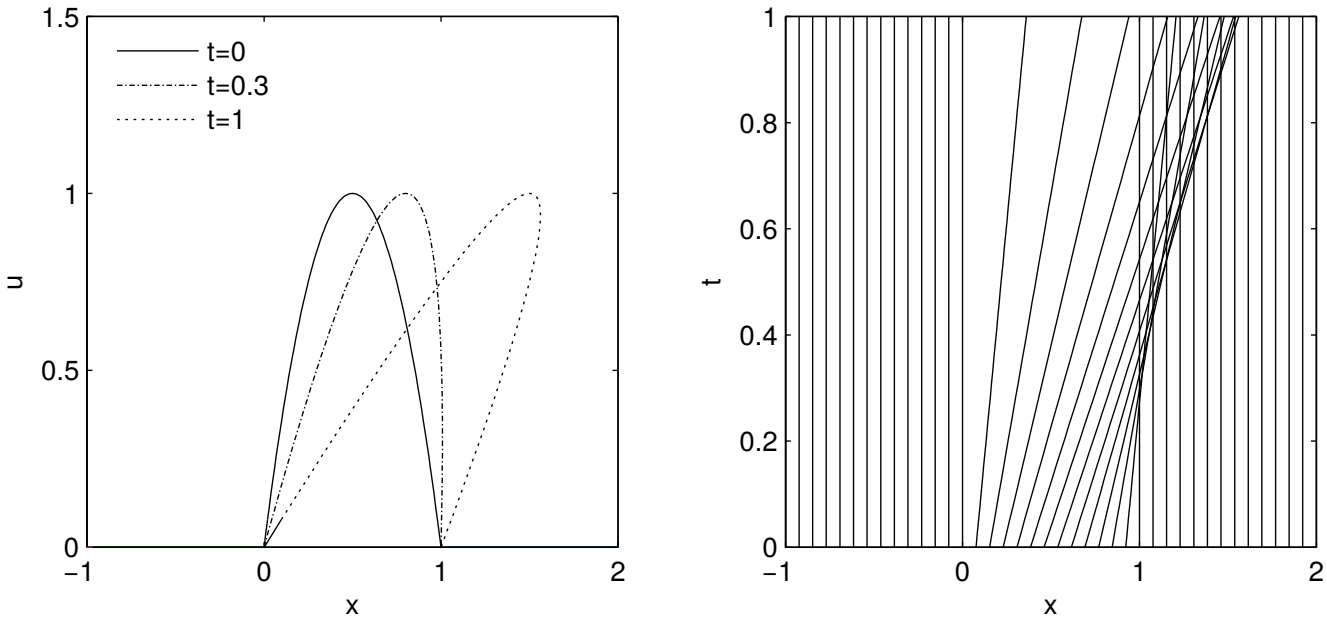

Figure 2.2: (Left) Initial condition and solution of Burgers equation at $t = 0.3$, and $t = 1$. (Right) Characteristic lines on which the solution is constant.

longer unique (at some positions in space there are two values of u). This can also be seen in the right graph were characteristic lines cross. Clearly something has gone wrong, because for a physical problem there can only be one solution. The problem appears when the lines starts to intersect. At this time the derivative is ill–defined and hence (2.14) is not valid. Keep in mind that the Burgers equation we wrote is a special case of the more general integral version and for this equation there are no problems with discontinuities. The problem of finding what the correct behavior at these discontinuities is called the Riemann problem, and solving it is the key to good numerical methods for hyperbolic systems.

2.3 The Riemann Problem

We saw in the previous section that the method of characteristics works well until the lines start intersecting. At this point a discontinuity forms and things start to go wrong. Before this time and for characteristic solutions that have not intersected yet, there is no problem. Our problem is thus only dealing with the discontinuity. A model problem with the same difficulty is the Riemann Problem (for a illustration see Figure 2.3)

$$\left.\begin{array}{l} \mathbf{U}_t + (\mathbf{F}(\mathbf{U}))_x = 0, \\ \mathbf{U}(x,0) = \left\{ \begin{array}{ll} \mathbf{U}_L & x < 0 \\ \mathbf{U}_R & 0 \leq x \end{array} \right. \end{array}\right\} \tag{2.16}$$

A possible solution to the problem, is for the discontinuity to move without change in form, this referred

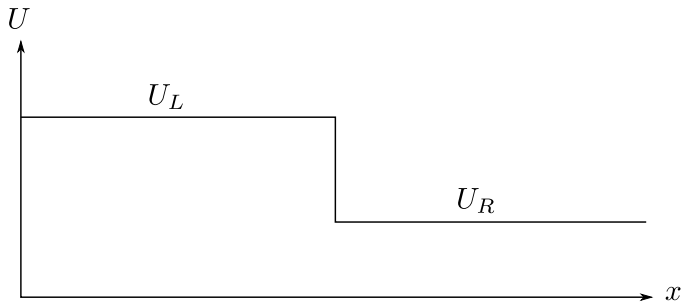

Figure 2.3: Illustration of the Riemann problem.

to as a shock. Using the integral formulation, we can derive the speed s with which this discontinuity should travel (also called the Rankine-Hugoniot conditions). The speed and conditions are derived by integrating (2.1) over $[x_-, x_+]$ $(x_- < 0 < x_+)$

$$\frac{\partial}{\partial t}\int_{x_-}^{x_+} \mathbf{U}\mathrm{d}x + \mathbf{F}(\mathbf{U}_R) - \mathbf{F}(\mathbf{U}_L) = 0, \tag{2.17}$$

$$\frac{\partial}{\partial t}\left(\mathbf{U}_L \cdot (x_{\text{shock}} - x_-) + \mathbf{U}_R \cdot (x_+ - x_{\text{shock}})\right) = -\left(\mathbf{F}(\mathbf{U}_L) - \mathbf{F}(\mathbf{U}_R)\right) \tag{2.18}$$

$$\tag{2.19}$$

giving the Rankine Hugoniot conditions

$$(\mathbf{U}_L - \mathbf{U}_R)s = -\left(\mathbf{F}(\mathbf{U}_L) - \mathbf{F}(\mathbf{U}_R)\right) \tag{2.20}$$

where $s \equiv \partial x_{\text{shock}}/\partial t$. Note that s has to satisfy this equation for all components. We now look at some specific examples of this.

Scalar In the scalar case we are left with the shock satisfying the following condition

$$s = \frac{f(U_R) - f(U_L)}{U_R - U_L}. \tag{2.21}$$

For the advection equation ($f(U) = au$) we have

$$s = \frac{aU_R - aU_L}{U_R - U_L} = a. \tag{2.22}$$

Not surprisingly the shock moves at the advection speed a. For the Burgers equation (2.14)

$$s = \frac{\frac{1}{2}U_R - \frac{1}{2}U_L}{U_R - U_L} = \frac{1}{2}\left(U_R + U_L\right), \tag{2.23}$$

i.e. the arithmetic average of the two velocities. Coincidentally, if $U_L > U_R > 0$ the solution will be

$$U(x,t) = \begin{cases} U_L & x < st \\ U_R & st \leq x \end{cases}. \tag{2.24}$$

Linear system For a linear system we have that $\mathbf{F}(\mathbf{U}) = \mathbf{A}\mathbf{U}$ and

$$\mathbf{A}\left(\mathbf{U}_R - \mathbf{U}_L\right) = s\left(\mathbf{U}_R - \mathbf{U}_L\right). \tag{2.25}$$

Thus for a linear system one may interpret s and

$$\Delta\mathbf{U} = \mathbf{U}_R - \mathbf{U}_L \tag{2.26}$$

as being eigenvalue and eigenvector of $\mathbf{A}$. Thus the shock moves at the same speed as one of the eigenvalues. This is exactly what we see for the scalar advection equation where the shock speed is equal to a.

So far we have stressed that from the integral formulation of conservation laws, one may obtain solutions that allow for discontinuities and we have obtained the speed at which these discontinuities travel. However, in using the integral formulation great care needs to be taken. Unlike for the partial differential formulation, this formulation does not have an unique solution, but many weak solutions. The challenge of the Riemann problem becomes then to find which solution corresponds to the physical solution (also referred to as the strong solution). A guiding principle for finding which of the solutions is the correct one is obtained by adding a small amount of viscosity. For the Burgers equation this is done as follows

$$u_t + (\frac{1}{2}u^2)_x = \nu u_{xx}. \tag{2.27}$$

This equation can no longer have discontinuities. Taking the limit at which $\nu \to 0$ we obtain the true solution[3]. In practice, adding viscosity in such a way for systems is a cumbersome way to find the right

[3]Numerical techniques for solving such problems often introduce such viscosity, this helps to explain why methods with large viscosity (like Lax–Friedrichs) converge to the correct solution.

solution as it will make already complex problems even more complex. However, we can show that this is equivalent to the method of choice, which is to check if the solution obeys the *Entropy conditions*. This method originates from the Euler equations, where the correct solution to the Riemann problem was determined by finding which solution decreases the entropy of the system. For a scalar quadratic ($f'(U) > 0$) conservation law we have the Lax entropy conditions: A shock is the correct solution given that

$$f'(U_L) > s > f'(U_R). \tag{2.28}$$

That is if the left side of the discontinuity has a higher characteristic speed than the shock speed and the shock speed has a higher speed than the right side, then the solution will be a shock. Let's go back to the Burgers equation. We have that $s = (U_R + U_L)$, and thus we have for a discontinuity the following cases

$$U_L < s < U_R, \tag{2.29}$$
$$U_L > s > U_R. \tag{2.30}$$

$U_R < U_L$ satisfies the entropy condition and thus for this case we get a shock. As $U_L < U_R$ does not satisfy (2.28), this means that a shock is not a physical solution. In this case the physical solution is the rarefaction wave solution shown in Figure (2.4). Why this is the correct solution can be seen by considering vanishing viscosity. If we have viscosity we expect the discontinuity to be of finite width. Drawing the characteristics we see that there is no intersection of lines. Taking the limit of vanishing viscosity we get the rarefaction wave shown in Figure (2.4). Note that this would not be possible for $U_L > U_R$ where we would get intersection of lines.

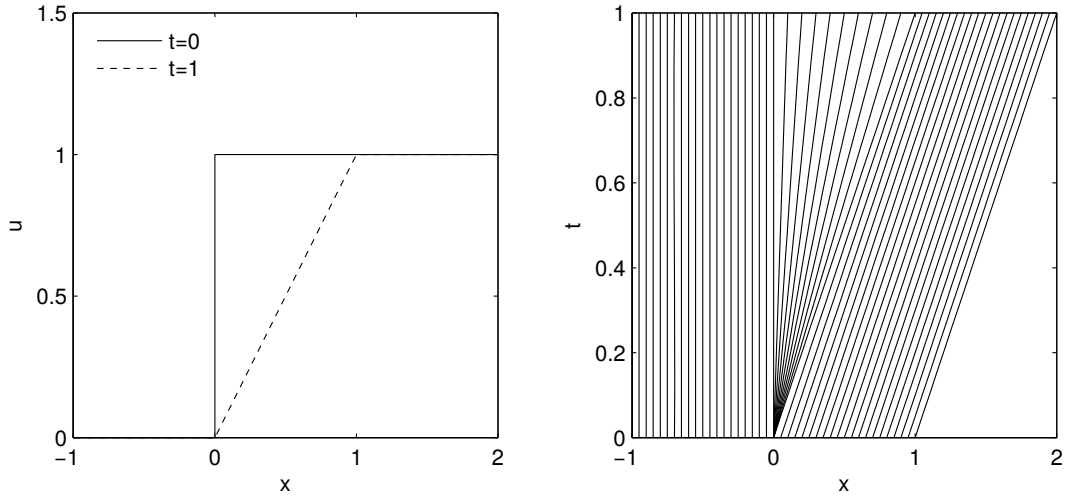

Figure 2.4: Illustration of rarefaction.

We have in this discussion not treated in detail a nonlinear system of conservation equations. Instead we have focused on linear systems and nonlinear scalar equations. Solving the Riemann problem for nonlinear systems is of course more difficult. However the general behavior can to a large degree be understood as a combination of the two.

3 The Finite volume method

Beyond linear system or scalar conservation laws, analytic treatment of hyperbolic problems becomes difficult if not impossible. To treat such problems further numerical methods are needed, and in this report we will focus on the *finite volume method* (FVM). In the 1D–FVM we consider a 1D conservation law on a line. We divide this line into N cells of width Δx, with center position x_i (see Figure). We are interested in finding the time evolution of the average amount of $\mathbf{U}$ on each piece. This is obtained by

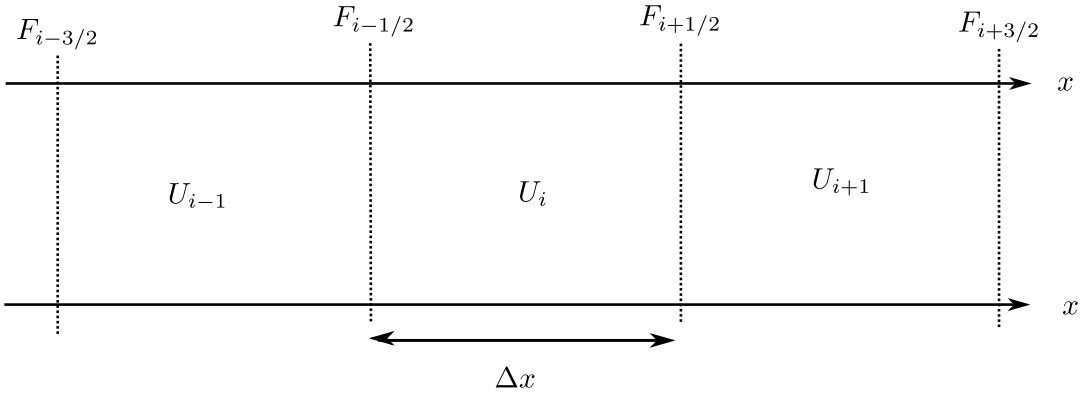

Figure 3.1: Finite volume computational grid.

integrating (2.1) over time from t_n to $t_{n+1} = t_n + \Delta t$ as follows

$$\int_{t_n}^{t_n+\Delta t} \mathrm{d}t \left(\int_{x_{i-1/2}}^{x_{i+1/2}} \frac{\partial \mathbf{U}}{\partial t} \mathrm{d}x + \mathbf{F}(\mathbf{U})_{i+1/2} - \mathbf{F}(\mathbf{U})_{i-1/2} \right) = 0,$$

integrating over time and space we find that

$$\hat{\mathbf{U}}_i^{n+1} - \hat{\mathbf{U}}_i^n + \frac{\Delta t}{\Delta x} \left(\hat{\mathbf{f}}_{i+1/2}^n - \hat{\mathbf{f}}_{i-1/2}^n \right) = 0, \tag{3.1}$$

where we used the following definitions

$$\hat{\mathbf{U}}_i^n \equiv \frac{1}{\Delta x} \int_{x_{i-1/2}}^{x_{i+1/2}} \mathbf{U}(x_i, t_n) \mathrm{d}x, \tag{3.2a}$$

$$\hat{\mathbf{f}}_{i\pm1/2}^n \equiv \frac{1}{\Delta t} \int_{t_n}^{t_n+\Delta t} \mathbf{F}(\mathbf{U}(x_{i\pm1/2}, t)) \mathrm{d}t. \tag{3.2b}$$

Equation (3.1) tells us that the change in average conserved quantity $\hat{\mathbf{U}}_i$ is equal to the average flux in and out at the boundary of the cell from time t_n to $t_n + \Delta t$. The goal of the Finite volume method is to find good approximations to $\hat{\mathbf{f}}_{i\pm1/2}$. There are two challenges to this. Firstly the fluxes are computed on the cell edges not inside the cells. Secondly these values change during the time integration.

Before going into specific methods we give some general remarks on the FVM.

Remark 1: Conservative method As we derived the method from the conservation equation the method is conservative. This can be shown by summation over the whole computational domain as follows

$$\Delta \mathbf{U}_{\text{tot}} = \sum_{i=1}^{N} (\hat{\mathbf{U}}_i^{n+1} - \hat{\mathbf{U}}_i^n) = -\frac{\Delta t}{\Delta x} \sum_{i=1}^{N} (\hat{\mathbf{f}}_{i+1/2}^n - \hat{\mathbf{f}}_{i-1/2}^n) = -\frac{\Delta t}{\Delta x} \left(\hat{\mathbf{f}}_{N+1/2}^n - \hat{\mathbf{f}}_{1/2}^n \right),$$

The change $\Delta \mathbf{U}_{\text{tot}}$ is equal to the total amount of flux going out at the right boundary minus the flux coming in at the left boundary. Methods where the flux is written in a consistent manner (the flux of left cell for the right cell border equals the flux for the right cell at left cell border) are always conservative.

Remark 2: Weak solutions We could have started from the differential equation formulation and easily derived finite difference methods. However, we saw that a partial differential formulation had problems treating shocks. Only using the integral formulation, we were able to treat these shocks. In the same way a great advantage of the FVM is that it being derived from the integral formulation we are able to describe these discontinuous solutions. Note how well these are approximated depend on how $\hat{\mathbf{f}}_{i\pm1/2}$ is approximated.

Remark 3: Close relationship to the Riemann problem By doing cell averages, we go from a smooth configuration Figure 3.2 (Left) into discrete values shown in Figure 3.2 (Right). At cell edges, where fluxes are computed $\mathbf{U}$ can take two values. Zooming in on two consecutive cells we see that the problem we are dealing with is the Riemann problem. Solving it yields the value of $\mathbf{U}$ during the time step at the edge and hence the average flux at the cell edge. How we solve or approximate this problem is what distinguishes between the different FVMs.

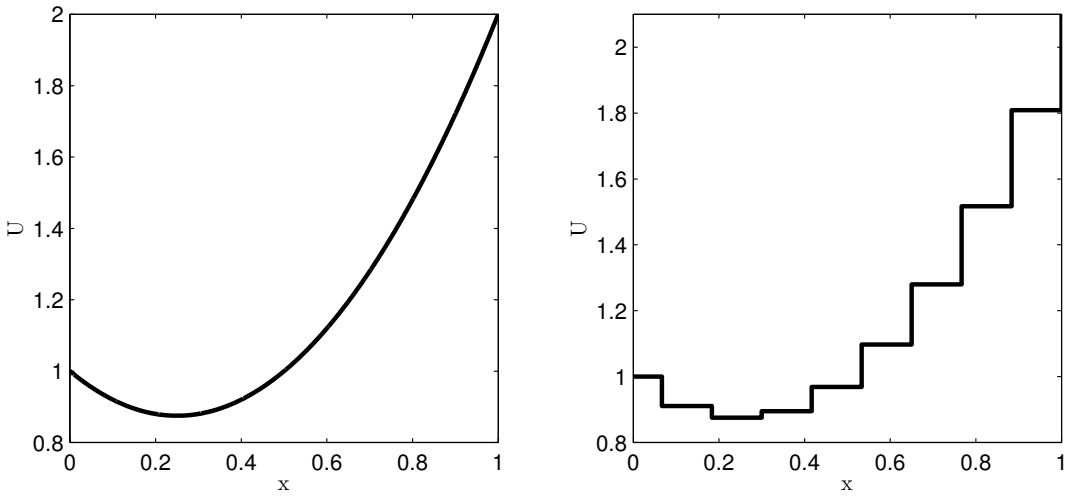

Figure 3.2: (Left) Smooth configuration. (Right) Cell average configuration.

Remark 4: Domain of dependence and domain of influence For hyperbolic conservation laws, solution or information travels at finite speeds given by the eigenvalues. This means that if points are far enough from each other they cannot interact. For instance for the linear conservation law and the point (x,t) the domain of dependence is given by

$$D = \{x - \lambda^p t, \quad p = 1, \ldots, n\}, \tag{3.3}$$

only these points will decide the solution at (x,t). Similarly, a point at (x,t) has a domain of influence

$$I = \{x + \lambda^p t, \quad p = 1, \ldots, n\}. \tag{3.4}$$

For a nonlinear conservation law, eigenvalues will depend on $\mathbf{U}$ and the domain of dependence and influence will be a bounded area rather than a set of points. Most FVMs only consider two cells per edge. For this to be correct one needs to make sure that information does not travel beyond one cell. The simplest example is shown in Figure 3.3 for the advection equation. Here the time step is chosen low enough so that cells only can influence neighboring cells. This limitation on the time step is called the CFL–condition. For a system of equations this can be generalized to

$$\frac{\max\left(\lambda_i\right)\Delta t}{\Delta x} < 1, \tag{3.5}$$

or the time step needs to be limited so that the distance the fastest information travels is less than the cell width. Note that the CFL–condition is a necessary condition for stability, however it is not sufficient. Individual methods and problems can require a smaller time steps than that of the CFL–condition for the FVM to be stable.

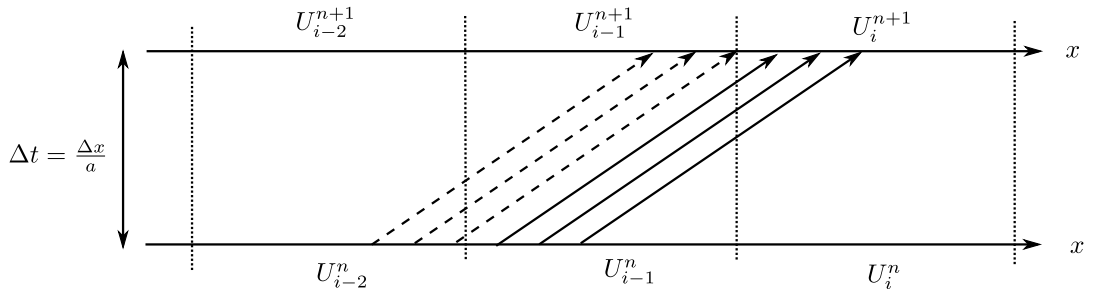

Figure 3.3: Illustration of the CFL–condition.

3.1 The Godunov Method

In the Godunov method [4] we solve the Riemann problem exactly at each edge and use the solution to compute $\hat{\mathbf{f}}(\mathbf{U}^n_{i\pm1/2})$. In the Godunov method this value is given by

$$\hat{\mathbf{f}}(\mathbf{U}) \simeq f(\mathbf{U}_\downarrow), \tag{3.6}$$

where $\mathbf{U}_\downarrow$ is value of $\mathbf{U}$ at the position of the edge during the time step. This process is visualized in Figure 3.4. Here we have two Riemann problems between two cells. In the left Figure the solution is a shock while in the right Figure the solution is a rarefaction fan. Despite this difference, in both situations during the whole time step, we have that the solution at $x = 0$ is given by $U_\downarrow = U_L$. Using this value in the flux we obtain the Godunov method in both cases. For a nonlinear system the solution is obtained

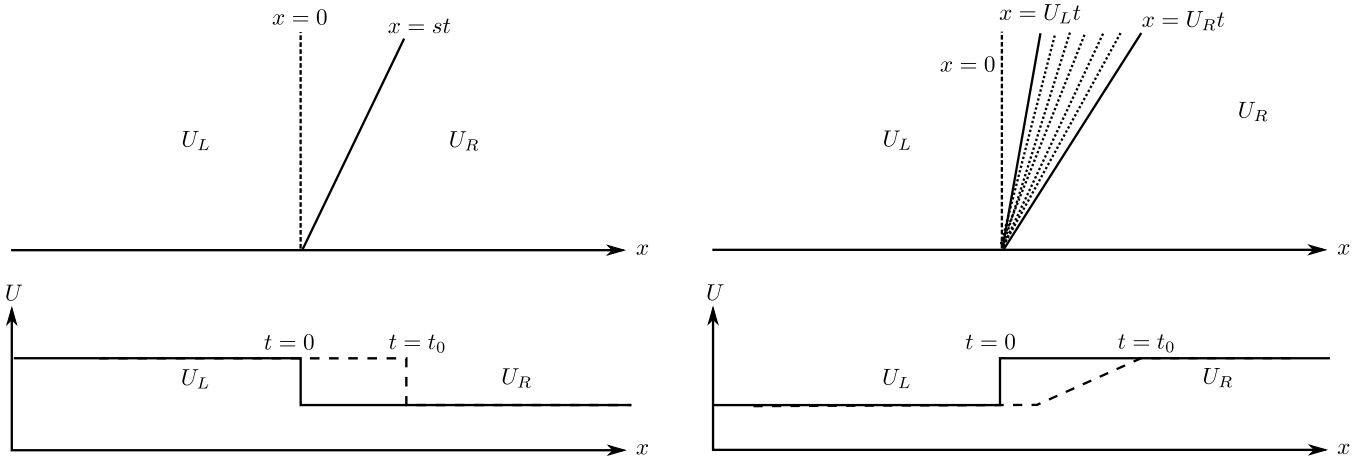

Figure 3.4: Illustration of how FVM works for the Godunov–method for two Riemann problems. (Left) We have a shock moving to the right, we see as time goes, the value of the edge ($x = 0$) is given by $U_\downarrow = U_L$. (Right) Example with left moving rarefaction, also in this case $U_\downarrow = U_L$.

in the same way by solving the Riemann problem exactly. If this cannot be done analytically, then it is done numerically, for instance by Newton's method. This can be very costly. Another approach is to solve the Riemann problem approximately. Many techniques are based on linearization of the system. That is to assume

$$\mathbf{F}(\mathbf{U}) \simeq \tilde{\mathbf{A}}\mathbf{U}, \tag{3.7}$$

where $\tilde{\mathbf{A}}$ depends on which approximate solver is used. The problem is then solved using the Godunov method as if the problem was linear. Motivated by this we seek a method for linear systems that is

$$\mathbf{F}(\mathbf{U}) = \mathbf{A}\mathbf{U}.$$

Since the system is linear we have that all cells share the same eigenvectors $\mathbf{r}^p$. This implies that

$$\mathbf{U}_i - \mathbf{U}_{i-1} = \sum_{p=1}^{m} \beta_i^p \mathbf{r}^p - \sum_{p=1}^{m} \beta_{i-1}^p \mathbf{r}^p = \sum_{p=1}^{m} (\beta_i^p - \beta_{i-1}^p)\mathbf{r}^p = \sum_{p=1}^{m} \alpha_{i-1/2}^p \mathbf{r}^p = \sum_{p=1}^{m} \mathbf{W}_{i-1/2}^p, \tag{3.8}$$

thus we have decomposed the discontinuity into waves $\mathbf{W}^p_{i-1/2}$. To each wave there corresponds a λ^p – the speed at which the wave travels. How each wave $\mathbf{W}^p_{i-1/2}$ affects neighboring cells can be understood by interpreting the Godunov method in terms of projection. Suppose we instead had a scalar system (see Figure 3.5) and that the eigenvalue is given by $a > 0$. The discontinuity wave will move into the

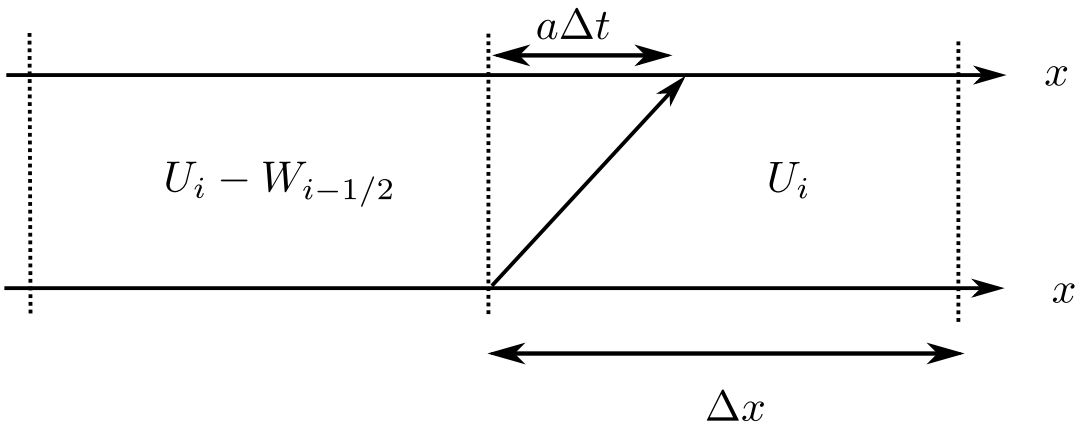

Figure 3.5: Illustration of projection–Godunov interpretation.

right cell and cover a portion $a\Delta t$ thereby changing it from $U_i \to U_i - W_{i-1/2}$. The remaining part of the cell is unaffected. Averaging or projecting the solution we obtain the following

$$U_i^{n+1} = U_i^n \frac{\Delta x - a\Delta t}{\Delta x} + (U_i^n - W_{i-1/2}) \frac{a\Delta t}{\Delta x},$$

or

$$U_i^{n+1} - U_i^n + \frac{a\Delta t}{\Delta x} W_{i-1/2} = 0. \tag{3.9}$$

For $a < 0$, cell i will only be affected by cell $i+1$ and we will have

$$U_i^{n+1} - U_i^n + \frac{a\Delta t}{\Delta x} W_{i+1/2} = 0. \tag{3.10}$$

This is easily generalized to any a as follows

$$U_i^{n+1} - U_i^n + \frac{\Delta t}{\Delta x}(a^+ W_{i-1/2} + a^- W_{i+1/2}) = 0, \tag{3.11}$$

where $a^+ = \max(a, 0)$ and $a^- = \min(a, 0)$. The same projection interpretation works for a system, however instead of one discontinuity wave there are multiple, each with its own advection speed. The generalization is straightforward

$$\mathbf{U}_i^{n+1} - \mathbf{U}_i^n + \frac{\Delta t}{\Delta x} \sum_{p=1}^{m} (\lambda_p^+ \mathbf{W}_{i-1/2} + \lambda_p^- \mathbf{W}_{i+1/2}) = 0. \tag{3.12}$$

In the literature this is also written as

$$\mathbf{U}_i^{n+1} - \mathbf{U}_i^n + \frac{\Delta t}{\Delta x} \sum_{p=1}^{m} (\mathcal{A}^+ \Delta \mathbf{U}_{i-1/2} + \mathcal{A}^- \Delta \mathbf{U}_{i+1/2}) = 0, \tag{3.13}$$

where

$$\mathcal{A}^\pm \Delta \mathbf{U}_{i\mp 1/2} = \sum_{p=1}^{m} \lambda_p^\pm \mathbf{W}_{i\mp 1/2}. \tag{3.14}$$

or

$$\mathbf{U}_i^{n+1} - \mathbf{U}_i^n + \frac{\Delta t}{\Delta x} \sum_{p=1}^{m} (\mathbf{A}^+ \Delta \mathbf{U}_{i-1/2} + \mathbf{A}^- \Delta \mathbf{U}_{i+1/2}) = 0, \tag{3.15}$$

because

$$A^\pm \boldsymbol{\Delta U}_\mp = \mathbf{R}\boldsymbol{\Lambda}^\pm \mathbf{R}^{-1} \boldsymbol{\Delta U}_\mp = \mathbf{R}\boldsymbol{\Lambda}^\pm \boldsymbol{\alpha}_{i\mp 1/2} = \sum_{p=1}^{m} \lambda_p^\pm \alpha_{i\mp 1/2}^p \mathbf{r}^p = \mathcal{A}^\pm \Delta \mathbf{U}_{i\mp 1/2}. \tag{3.16}$$

Remark When we say that we solve the Riemann–problem exactly using the Godunov–method this does not mean that our numerical method is exact. No matter how well the Godunov–method solves the Riemann problem, it still only considers only two cells and can only get first order accuracy. To obtain higher accuracy extrapolation from next neighboring cells needs to be used. However this must be done with care using *limiters* as straightforward extrapolations will lead to large oscillations near the discontinuities. For a thorough treatment of this we refer to [5].

3.2 Approximate methods

To apply the Godunov method on a system of equations we only need to determine $\mathbf{U}_\downarrow$, for each Riemann problems. In doing so we also compute the whole structure of the Riemann problem, whether or not we have shocks or rarefaction waves. However, in most cases $\mathbf{U}_\downarrow$ lies somewhere in the intermediate states in between shocks and rarefaction waves. A good example of this is shown in figure 3.4, where the value of $\mathbf{U}_\downarrow$ is independent of if we have rarefaction or not. Only for transonic rarefaction (a rarefaction fan spanning from left to right) will we need the to know the details. Thus in most cases a lot of detailed information is obtained without being used. Approximate Riemann solvers can reduce the number of costly computations and in many cases obtain the exact same result as Godunov. We will in this section go through the approximate Riemann solvers we will use for our model system.

3.2.1 Lax–Friedrichs

One of the simplest and most robust approximate Riemann solver is the Lax–Friedrichs. In this scheme we approximate $\hat{\mathbf{f}}(\mathbf{U})$ by

$$\mathbf{f}_{i-1/2}^{(LF)} = \frac{1}{2}\left(\mathbf{f}(\mathbf{U}_{i-1}) + \mathbf{f}(\mathbf{U}_i)\right) - \frac{\Delta x}{2\Delta t}\left(\mathbf{U}_i - \mathbf{U}_{i-1}\right), \tag{3.17}$$

giving the following method

$$\mathbf{U}_i^{n+1} - \mathbf{U}_i^n + \frac{\Delta t}{2\Delta x}\left(\mathbf{f}(\mathbf{U}_{i+1}) + \mathbf{f}(\mathbf{U}_{i-1})\right) - \frac{1}{2}\left(\mathbf{U}_{i+1} + \mathbf{U}_{i-1} - 2\mathbf{U}_i\right) = 0. \tag{3.18}$$

We can show that the method is consistent by Taylor expansion, this gives

$$\frac{\partial \mathbf{U}}{\partial t} + \frac{\partial \mathbf{f}(\mathbf{U})}{\partial x} = \frac{\Delta x^2}{2\Delta t}\frac{\partial^2 \mathbf{U}}{\partial x^2} + \mathcal{O}(\Delta t), \tag{3.19}$$

a convection–diffusion equation. However we have an upper CFL–condition for the ratio $\Delta x/\Delta t$, and thus the diffusion term is $\mathcal{O}(\Delta x)$. With grid refinement this term will disappear and the method is thus consistent. The viscous part works in the same way as an entropy condition making sure we always obtain the correct solution to the Riemann problem. Lax–Friedrichs is thus very robust, but also tends to smear out the solutions. Because of it is simplicity and robustness, it is very useful as a first approach. However, due to its smearing, other methods are generally preferred.

3.2.2 HLLC method

In our discussion of linear conservation laws we saw that the initial discontinuity of the Riemann problem $\Delta\mathbf{U}$ separated into waves $\mathbf{W}^p$ traveling at a characteristic speeds λ^p. Thus a single discontinuity is transformed into multiple discontinuities. Similarly we have the same behavior for nonlinear systems, but with added complexity of rarefaction waves and shocks. In most cases $\mathbf{U}_\downarrow$ will be at one of these levels. In the model system we have six variables, but only three characteristic velocities (see Appendix A.2) $\{u-c, u, u+c\}$ (second speed is 4–degenerate). This means that for our model system there can be a maximum of three shocks, contact discontinuity and rarefaction waves, which gives a total of four separate states. A method that is very good for such problems is the HLLC method [9]. In the HLLC–method the discontinuity of the Riemann problem is allowed to separate into three discontinuities, the speeds of which are given by the slowest speed S_L a middle speed S_* and the fastest speed S_R as illustrated in figure 3.6. Assuming that the Riemann problem solution has this structure we derive the conditions for the speeds and the separate states. We start off by considering a Riemann problem contained in the control volume $[x_L, x_R] \times [0, T]$

$$\left.\begin{array}{l} \mathbf{U}_t + \mathbf{F}(\mathbf{U})_x = 0 \\ \mathbf{U}(x,0) = \left\{ \begin{array}{lll} \mathbf{U}_L & \text{if} & x \le 0 \\ \mathbf{U}_R & \text{if} & x \ge 0 \end{array} \right. \end{array}\right\} \tag{3.20}$$

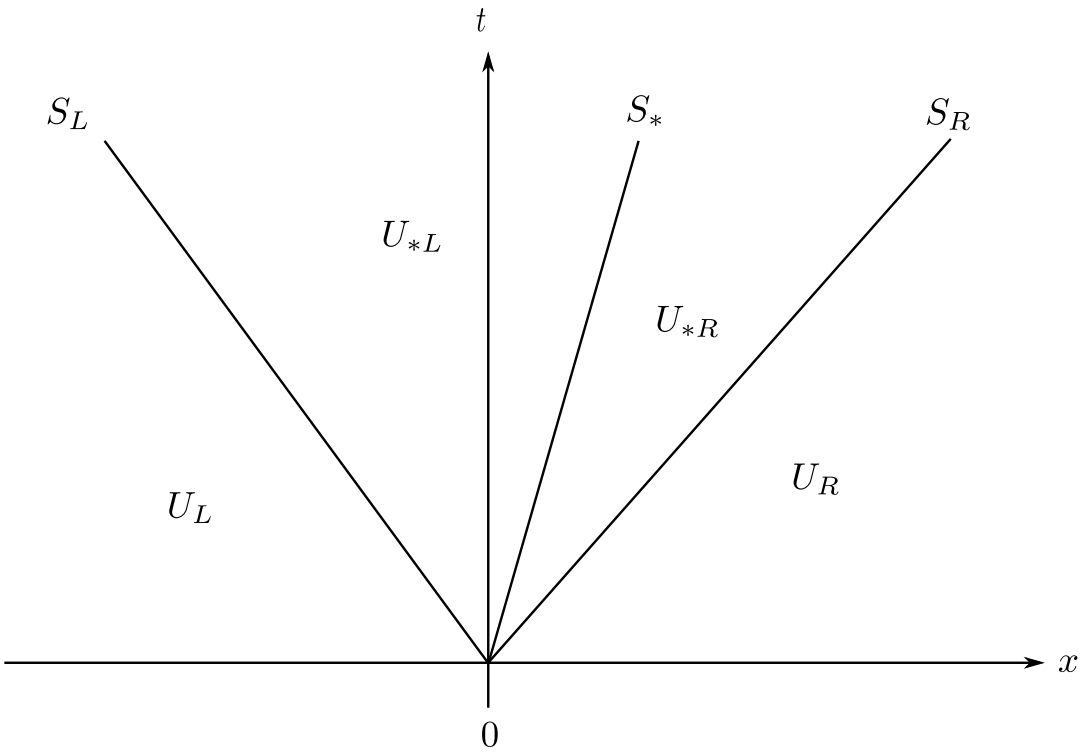

Figure 3.6: Illustration of HLLC–separation into four states.

integrating over the control volume and time we find the following consistency condition

$$\int_{x_L}^{x_R} \mathbf{U}(x,T)\mathrm{d}x = \int_{x_L}^{x_R} \mathbf{U}(x,0)\mathrm{d}x + \int_0^T \mathbf{F}(U(x_L,t)\mathrm{d}t - \int_0^T \mathbf{F}(U(x_R,t)\mathrm{d}t \tag{3.21}$$

$$= x_R\mathbf{U}_R - x_L\mathbf{U}_L + T(\mathbf{F}_L - \mathbf{F}_R). \tag{3.22}$$

Using the separation shown in figure 3.6 this should be equal to

$$\int_{x_L}^{x_R} \mathbf{U}(x,T)\mathrm{d}x = \int_{x_L}^{TS_L} \mathbf{U}(x,T)\mathrm{d}x + \int_{TS_L}^{TS_*} \mathbf{U}(x,T)\mathrm{d}x + \int_{TS_*}^{TS_R} \mathbf{U}(x,T)\mathrm{d}x + \int_{TS_R}^{x_R} \mathbf{U}(x,T)\mathrm{d}x \tag{3.23}$$

$$= \int_{TS_L}^{TS_*} \mathbf{U}(x,T)\mathrm{d}x + \int_{TS_*}^{TS_R} \mathbf{U}(x,T)\mathrm{d}x + (TS_L - X_L)\mathbf{U}_L + (x_R - TS_R)\mathbf{U}_R \tag{3.24}$$

Setting (3.22) and (3.24) equal we obtain a the consistency condition for the HLLC–method

$$\frac{S_* - S_L}{S_R - S_L}\mathbf{U}_{*L} + \frac{S_R - S_*}{S_R - S_L}\mathbf{U}_{*R} = \frac{S_R\mathbf{U}_R - S_L\mathbf{U}_L + \mathbf{F}_L - \mathbf{F}_R}{S_R - S_L}, \tag{3.25}$$

where we defined

$$\mathbf{U}_{*L} = \frac{1}{T\,(S_* - S_L)} \int_{TS_L}^{TS_*} \mathbf{U}(x,T)\mathrm{d}x, \tag{3.26}$$

$$\mathbf{U}_{*R} = \frac{1}{T\,(S_R - S_*)} \int_{TS_*}^{TS_R} \mathbf{U}(x,T)\mathrm{d}x. \tag{3.27}$$

The solution of the Riemann problem then becomes

$$\mathbf{U}^{\mathrm{HLLC}}(x,t) = \begin{cases} \mathbf{U}_L, & \text{if} \quad x/t \le S_L \\ \mathbf{U}_{*L}, & \text{if} \quad S_L \le x/t \le S_* \\ \mathbf{U}_{*L}, & \text{if} \quad S_* \le x/t \le S_R \\ \mathbf{U}_R, & \text{if} \quad S_R \le x/t \end{cases}, \tag{3.28}$$

or in terms of fluxes

$$\mathbf{F}^{\mathrm{HLLC}}_{i-1/2} = \begin{cases} \mathbf{F}_L, & \text{if} \quad 0 \le S_L \\ \mathbf{F}_{*L}, & \text{if} \quad S_L \le 0 \le S_* \\ \mathbf{F}_{*R}, & \text{if} \quad S_* \le 0 \le S_R \\ \mathbf{F}_R, & \text{if} \quad S_R \le 0 \end{cases} \tag{3.29}$$

To determine F_{*L} and F_{*R} we impose the Rankine–Hugoniot conditions

$$\mathbf{F}_{*L} - \mathbf{F}_L = S_L \left(\mathbf{U}_{*L} - \mathbf{U}_L\right), \tag{3.30}$$
$$\mathbf{F}_{*R} - \mathbf{F}_{*L} = S_* \left(\mathbf{U}_{*R} - \mathbf{U}_{*L}\right), \tag{3.31}$$
$$\mathbf{F}_R - \mathbf{F}_{R*} = S_R \left(\mathbf{U}_R - \mathbf{U}_{*R}\right). \tag{3.32}$$

Inserting one into the other one can show that these three equations also contain (3.25), thus we have four unknowns and three equations. This might seem as a problem, but it is actually the opposite. This freedom allows us to put additional constraint which we see fit.

When using the HLLC–Riemann solver we can directly insert (3.29) into the Godunov method. An equivalent approach is a wave formulation similar to what we did for the linear system, only we have three waves $\Delta\mathbf{U}^p = \{\mathbf{U}_{*L} - \mathbf{U}_L, \mathbf{U}_{*R} - \mathbf{U}_{*L}, \mathbf{U}_R - \mathbf{U}_{*R}\}$ traveling at speeds $S_p = \{S_L, S_*, S_R\}$. The HLLC–method then becomes

$$\mathbf{U}_i^{n+1} - \mathbf{U}_i^n + \frac{\Delta t}{\Delta x} \sum_{p=1}^{3} \left(S^p_{i-1/2}\right)^+ \Delta\mathbf{U}^p_{i-1/2} + \left(S^p_{i+1/2}\right)^- \Delta\mathbf{U}^p_{i+1/2}) = 0. \tag{3.33}$$

3.2.3 Roe Method

We have seen previously that it is sometimes useful to express the hyperbolic conservation laws in quasilinear form

$$\mathbf{U}_t + \mathbf{A}(\mathbf{U})\mathbf{U}_x = 0, \tag{3.34}$$

where

$$\mathbf{A}\left(\mathbf{U}\right) = \frac{\partial \mathbf{F}}{\partial \mathbf{U}} \tag{3.35}$$

is the Jacobi matrix. We saw previously that for a linear system we can easily solve the Riemann problem. In this spirit Roe [7] proposed to rather than approximating the flux, to approximate $\mathbf{A}(U)$ by a constant matrix $\tilde{\mathbf{A}}$ constant in time and then solve

$$\left.\begin{array}{l} \mathbf{U}_t + \tilde{\mathbf{A}}\mathbf{U}_x = 0 \\ \mathbf{U}(x,0) = \left\{ \begin{array}{lll} \mathbf{U}_L & \text{if} & x \le 0 \\ \mathbf{U}_R & \text{if} & x \ge 0 \end{array} \right. \end{array}\right\} \tag{3.36}$$

exactly for each edge. However, which value should we use: $\tilde{\mathbf{A}} = \mathbf{A}(\mathbf{U}_L)$ or $\tilde{\mathbf{A}} = \mathbf{A}(\mathbf{U}_R)$? Roe proposed to use an average or a combination of the two. Further he required this matrix to satisfy the following properties:

Porperty A: Hyperbolicity of the problem. This equivalent to require that $\tilde{\mathbf{A}}$ has only real eigenvalues and that all eigenvectors are linearly independent.

Porperty B: Consistency with the exact Jacobian

$$\tilde{\mathbf{A}}(\mathbf{U},\mathbf{U}) = \mathbf{A}(\mathbf{U}). \tag{3.37}$$

Property C: Conservation across discontinuities

$$\mathbf{F}(\mathbf{U}_R) - \mathbf{F}(\mathbf{U}_L) = \tilde{\mathbf{A}}(\mathbf{U}_R - \mathbf{U}_L). \tag{3.38}$$

Property (A) ensures us that the approximate Riemann problem has the same mathematical character as the one we are trying to approximate. Secondly it also guarantees that we can solve the problem using the wave structure. Property (B) ensures that our problem becomes consistent with our original problem. Property (C) ensures that the method is conservative.

The Roe–matrix will of course depend on the problem and is in general cumbersome to derive, especially if the problem is complicated (like for our model system). Assuming we have the Roe–matrix, we then automatically obtain the eigenstructure. Projecting the discontinuity onto waves $\mathbf{W}^p_{i-1/2}$ going at speed $\lambda^p_{i-1/2}$ we solve it by

$$\mathbf{U}_i^{n+1} - \mathbf{U}_i^n + \frac{\Delta t}{\Delta x} \sum_{p=1}^{m} \left(\left(\lambda^p_{i-1/2}\right)^+ \mathbf{W}^p_{i-1/2} + \left(\lambda^p_{i+1/2}\right)^- \mathbf{W}^p_{i+1/2} \right) = 0. \tag{3.39}$$

Note that we now use lower indcies on eigenvalues, because unlike for a linear system, the Roe–matrix is different at each edge. For some problems including our model, algebraic relations can be found for the eigenvaluee, strengths and eigenvectors. In doing so we save computing time that would have gone into the system and computing eigenvalues and vectors numerically. In doing so we avoid computation of the Roe–matrix altogether.

4 Relaxation systems

In nature we are often faced with systems in which there is an equilibrium relationship between the variables. Whenever the system is perturbed from equilibrium the system will seek to restore equilibrium and the process by which this happens is called *relaxation*. To model such systems we generalize our conservation law to

$$\mathbf{U}_t + \mathbf{F}(\mathbf{U})_x = \frac{1}{\epsilon}\mathbf{R}(\mathbf{U}), \tag{4.1}$$

where the right side is the hyperbolic conservation law and on the left side $\mathbf{R}(\mathbf{U})$ is the equilibrium relationship, and ϵ the time scale at which the system relaxes towards equilibrium. This extension adds an equilibrium relationship to the model and models the process by which this happens. An example of such a term can be seen in our model: The ψ source term which relaxes the different pressures of the two phases. In this case, relaxation is modeled to happen through changes in volume fraction of the two phases and through the associated energy exchange.

Relaxation typically happens in a short time scale and the relaxation term will become big whenever the system is perturbed from equilibrium, making such terms stiff. To account for such terms numerically for arbitrary relaxation times, special care needs to be taken. Here we present some options for dealing with such terms assuming fractional step, and an equation of the form

$$\mathbf{U}_t = \frac{1}{\epsilon}\mathbf{R}(\mathbf{U}). \tag{4.2}$$

4.1 Infinitely fast relaxation

A popular way of dealing with relaxation is to take the limit of $\epsilon \to 0$, corresponding to instantaneous relaxation. In this limit the system will relax fully during the time step and

$$\mathbf{U}^{n+1} \simeq \mathbf{U}^{eq}, \tag{4.3}$$

the equilibrium value after relaxation. Thus, to use this method we only need to compute the equilibrium value. This method is both fast, robust and simple. However it assumes very fast relaxation, and for some problems relaxation process might be slow and a part of the physics we want to describe.

Remark An alternative way whenever relaxation is very fast is to enforce the equilibrium condition of $\mathbf{R}(\mathbf{U})$ onto the system of differential equation such that $\mathbf{R}(\mathbf{U}) = 0$ always. This will reduce the number of equations. In fact this type of relaxation is the link between the many two–phase models. One might think that it is always best to reduce the number of equations to the minimal as possible, thereby reducing complexity. However in doing it is sometimes harder to construct numerical techniques that respect conservation.

4.2 ASY–method

The ASY–method [1] is a relatively new method that was specifically designed for relaxation problems. In this method we assume that the system relaxes asymptotically in time towards the equilibrium value $\mathbf{U}^{eq}$. The ASY–method is given by

$$\left.\begin{aligned} \mathbf{U}_i^{n+1} &= \mathbf{U}_i^n + (\mathbf{U}_i^{eq} - \mathbf{U}_i^n)\left(1 - \exp\left(-\tfrac{\Delta t}{\tau_i}\right)\right) \\ \tau_i &= \epsilon \tfrac{\mathbf{U}_i^{eq} - \mathbf{U}_i^n}{\mathbf{R}(\mathbf{U}_i^n)} \end{aligned}\right\}. \tag{4.4}$$

For the method to be of any use it has to be convergent. This can be shown by proving the method is consistent and stable and then applying the Lax–equivalence theorem which states that convergence is equivalent to consistency and stability. First we show consistency by taking the limit[4] of $\Delta t \to 0$ and

[4] $\Delta t \ll \epsilon$

Taylor expansion

$$\mathbf{U}_i^{n+1} - \mathbf{U}_i^n = (\mathbf{U}_i^{eq} - \mathbf{U}_i^n)\left(1 - \exp\left(-\frac{\Delta t}{\tau_i}\right)\right)$$

$$\mathbf{U}_t\Delta t + \frac{1}{2}\mathbf{U}_{tt}\Delta t^2 + \mathcal{O}\Delta t^3 = (\mathbf{U}^{eq} - \mathbf{U})\left(1 - 1 + \frac{\Delta t}{\tau} - \frac{1}{2}\left(\frac{\Delta t}{\tau}\right)^2 + \mathcal{O}(\Delta t^3)\right)$$

$$\mathbf{U}_t\Delta t + \frac{1}{2}\mathbf{U}_{tt}\Delta t^2 + \mathcal{O}\Delta t^3 = (\mathbf{U}^{eq} - \mathbf{U})\left(\frac{\Delta t\mathbf{R}(\mathbf{U})}{\epsilon\,(\mathbf{U}^{eq} - \mathbf{U})} - \frac{1}{2}\left(\frac{\Delta t\mathbf{R}(\mathbf{U})}{\epsilon\,(\mathbf{U}^{eq} - \mathbf{U})}\right)^2 + \mathcal{O}(\Delta t^3)\right).$$

Finally, dividing by Δt we get

$$\mathbf{U}_t = \frac{1}{\epsilon}\mathbf{R}(\mathbf{U}) - \left(\frac{1}{2}U_{tt} + \frac{1}{\epsilon^2\,(\mathbf{U}^{eq} - \mathbf{U})}\mathbf{R}(\mathbf{U})^2\right)\Delta t + \mathcal{O}(\Delta t), \tag{4.5}$$

giving a convergent method when $\Delta t \to 0$. Note that there seems to be a problem for the consistency when $\epsilon \to 0$, however the more detailed analysis in [1] shows consistency for $\epsilon \to 0$.

A detailed analysis of stability is beyond the scope of this report (see [1]). However, a close look at figure 4.1 can shed some light into why it is stable. In this figure we see how the step is done by following an exponential that goes asymptotically towards the equilibrium value. No matter how long the time step and how many, the method cannot reach the equilibrium value, thus making it stable for any time step.

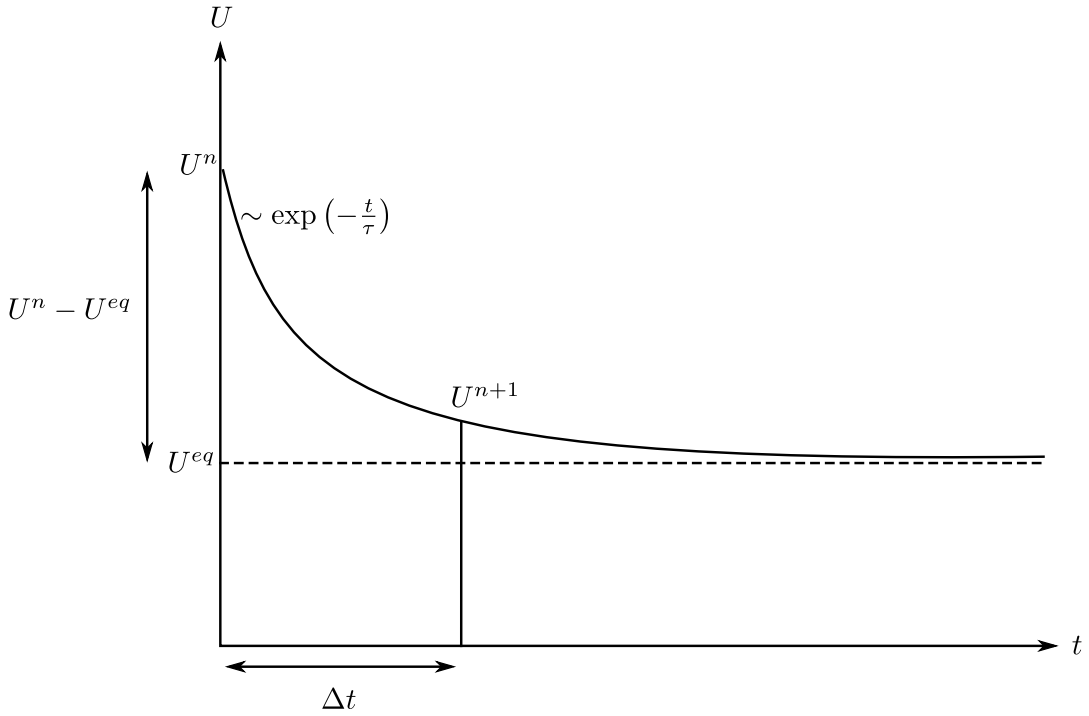

Figure 4.1: Illustration of how the ASY–method works.

Strengths and weaknesses There are many strengths to the ASY–method that makes it suitable for relaxation system. Firstly it is a very robust method. Not only is it stable for any time step, it also doesn't allow for overshoots. This can be seen from Figure 4.1 where no matter the length and number of time steps, we can never fully reach the equilibrium value and thus never pass it. This is very desirable as overshoots can result into nonphysical values, like negative pressure and mass fractions, which might lead to the simulation crashing. Another great strength is that the ASY–method becomes exact when we have exponential relaxation of the form

$$u_t = \frac{1}{\epsilon}(u_0^{eq} - u), \tag{4.6}$$

which is a very frequent form of relaxation. Thus in theory the method has few weaknesses. However there are some numerical issues for the actual implementation of the method when it comes to the limit $\mathbf{U} - \mathbf{U}^{eq} \to 0$. In this limit we run into problems in computing τ (assuming $\mathbf{R}(\mathbf{U}eq) = 0$) of form $0/0$, thereby crashing the program. One way of dealing with this problem is by adding if–statements to deal with $\mathbf{U} - \mathbf{U}^{eq} < \delta$, to ensure correct limit of $\mathbf{U}$ not changing. Another might be to add an machine–epsilon to the nominator and denominator in some fashion in order to avoid divergence. In any case, this is a complicating factor which adds complexity and can the reduce the efficiency of the ASY–method. When using ASY on a problem care needs to be taken. For it to work properly we need the following:

- Equilibrium has to be monotonically reached.
- Equilibrium value used needs to be the correct value.

If either of the two propperties are not met we can get negative τ and the exponential will easily diverge, leading to the program crashing.

ASY–method vs. implicit methods A very viable alternative to the ASY–method is an implicit method, for instance implicit Euler

$$\mathbf{U}^{n+1} = \mathbf{U}^n + \frac{1}{\epsilon}\Delta t \mathbf{R}(\mathbf{U}^{n+1}). \tag{4.7}$$

Like the ASY–method, it is stable for any time step and has no problem in dealing with stiff terms. It can have overshoots, but when this is not a problem, they have about the same robustness and their accuracy is $\mathcal{O}(\Delta t)$. Thus, their performance is similar, and not necessarily the deciding factor for which to use. In most cases the deciding factor is computing time. For the ASY–method, we need to compute the $\mathbf{U}^{eq}$ at each time step, while for the implicit Euler we need to solve (4.7) at each step. Which is fastest will depend on the problem. In some cases $\mathbf{U}^{eq}$ can be calculated analytically and ASY is then likely to outperform implicit Euler in speed. In other cases $\mathbf{U}^{eq}$ is not easily available and implicit Euler might be faster. Finally, we might be interested in increasing the order of accuracy. With the ASY–method, we can, by adding a few lines of code obtain second order accuracy, without calculating a new $\mathbf{U}^{eq}$. Using an implicit method (like second order implicit Runge Kutta) we have to further solve a second set of equations. Thus, an increased demand of accuracy can in some cases make the ASY–method the best choice.

4.3 Fractional step approach

For a general relaxation system we have to solve equations of the form

$$\frac{\partial \mathbf{U}}{\partial t} + \mathbf{A}(\mathbf{U})\mathbf{U}_x = \psi(\mathbf{U}), \tag{4.8}$$

most often the hyperbolic part of this equation operates at a slower time scale than that of the relaxation term, making this term stiff. For solving this equation numerically, there are three options. We can solve it with an explicit method, with a short enough time step to resolve the relaxation term in time. This is not practical, as the number of time steps needed becomes very large. It will also decrease the accuracy of the hyperbolic part, which starts to smear when time step becomes much smaller than the CFL–condition. A second option is to solve the whole equation implicitly. If implemented this would work and allow for large time steps. However, it would require us to solve a nonlinear system of equations. This will result in a much slower method, without adding much to the accuracy of the hyperbolic part, which is well treated by an explicit method. The third option, is the fractional step method, and is the one we will focus on in this report. In this method we combine the best features of the two methods above, explicit treatment of the hyperbolic part, and special treatment of the second part. Fractional step is illustrated in Figure 4.2. First we solve the hyperbolic part of the differential equation, obtaining $\mathbf{U}^*$. Then we solve the equation with relaxation with $\mathbf{U}^*$ as initial condition. A nice way of interpreting this approach, is that the hyperbolic part drives the system out of equilibrium, and the relaxation term tries to reinstate it afterwards.

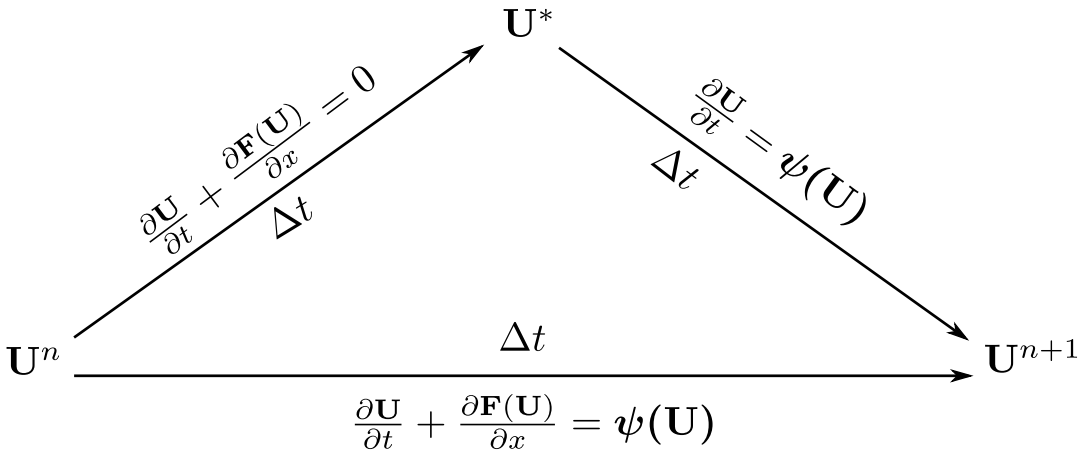

Figure 4.2: Illustration of the fractional step method.

5 Investigation of model system

In this section we will consider in more detail resolving the 6–equation 2–phase single velocity model with finite pressure relaxation. Until now we have been very general. This has helped to set our model system into a greater context. However, in doing so we have also ignored some of the intricacies of this specific model. Therefore we will in this section start by addressing these.

We recall the set of equations for the six–equation single–velocity model:

$$\partial_t \alpha_1 + \mathbf{u} \cdot \boldsymbol{\nabla} \alpha_1 = \mu \left(p_1 - p_2 \right) \tag{5.1a}$$
$$\partial_t (\alpha_1 \rho_1) + \boldsymbol{\nabla} \cdot (\alpha_1 \rho_1 \mathbf{u}) = 0 \tag{5.1b}$$
$$\partial_t (\alpha_2 \rho_2) + \boldsymbol{\nabla} \cdot (\alpha_2 \rho_2 \mathbf{u}) = 0 \tag{5.1c}$$
$$\partial_t (\rho \mathbf{u}) + \boldsymbol{\nabla} \cdot (\rho \mathbf{u} \otimes \mathbf{u}) + \boldsymbol{\nabla} \left(\alpha_1 p_1 + \alpha_2 p_2 \right) = 0 \tag{5.1d}$$
$$\partial_t \left(\alpha_1 E_1 \right) + \boldsymbol{\nabla} \cdot (\alpha_1 E_1 \mathbf{u} + \alpha_1 p_1 \mathbf{u}) + \Sigma(q, \boldsymbol{\nabla} q) = -\mu p_I (p_1 - p_2) \tag{5.1e}$$
$$\partial_t \left(\alpha_2 E_2 \right) + \boldsymbol{\nabla} \cdot (\alpha_2 E_2 \mathbf{u} + \alpha_2 p_2 \mathbf{u}) - \Sigma(q, \boldsymbol{\nabla} q) = \mu p_I (p_1 - p_2) \tag{5.1f}$$

As the equations stand now, there are not enough constraints on the system for closing this set of equations. We need a way of calculating the pressure given $\mathbf{U}$ (given in (1.7)). To do so we specify the equation of state.

5.1 Equation of state

In the following we will use *stiffened gas* (SG) as equation–of–state (EOS) independently for each phase. This EOS is a generalization of the ideal gas law by adding a stiffening parameter. Optimizing the parameters of the SG–EOS, this EOS not only models gasses, but may also model liquids and solids. The pressure and temperature in each phase is given by

$$p_k = (\gamma_k - 1)\rho_k (e_k - e_k^*) - \gamma_k \pi_k, \tag{5.2}$$
$$T_k = \frac{p_k + \pi_k}{C_{vk} \rho_k (\gamma_k - 1)} \tag{5.3}$$

where γ_k is the adiabatic ratio $\gamma = C_p / C_v$, e_k is the specific internal energy, e_k^* is the zero point specific energy and π_k is a parameter that stiffens the gas by increasing the sound velocity. For details on the SG–EOS the reader is referred to [3].

To close the system of equations we use that

$$\alpha_k E_k = \alpha_k \rho_k e_k + \frac{1}{2} \alpha_k \rho \mathbf{u}^2, \tag{5.4}$$

giving a direct link between thermodynamical variables like pressure and temperature to the "conserved variables"[5] of $\mathbf{U}$. How this is done is shown in Appendix A.1.

[5] Using the SG–EOS we could very well write (5.1) in terms of thermodynamical variables. However these are not conserved and will make it difficult to design numerical methods that conserve the conserved quantities.

5.2 Problem with non-conservative terms

The homogeneous part can be written as

$$\partial_t \mathbf{U} + \partial_x \mathbf{F}(\mathbf{U}) + \boldsymbol{\sigma}(\mathbf{U}, \partial_x \mathbf{U}) = 0, \tag{5.5}$$

right from the outset we see there is an immediate complication to our problem as $\boldsymbol{\sigma}$ is not of conservative form and is given by

$$\boldsymbol{\sigma}(\mathbf{U}) = \begin{pmatrix} \mathbf{u} \cdot \boldsymbol{\nabla} \alpha_1 \\ 0 \\ 0 \\ 0 \\ \Sigma(\mathbf{U}, \boldsymbol{\nabla}\mathbf{U}) \\ -\Sigma(\mathbf{U}, \boldsymbol{\nabla}\mathbf{U}) \end{pmatrix}. \tag{5.6}$$

In order to treat this term, the FVMs we introduced earlier need to be generalized. We will look at how this can be done on a case by case basis.

Lax–Friedrichs: The flux term is incorporated into the classical Lax–Friedrichs method. $\boldsymbol{\sigma}$ cannot be included into this. What we can do is to approximate the derivatives by a finite difference method. In our case we choose to approximate all derivatives of arbitrary quantities q by

$$\frac{\partial q_i}{\partial x} \simeq \frac{q_{i+1} - q_{i-1}}{2\Delta x}. \tag{5.7}$$

This is in the same spirit of how $\partial_x \mathbf{F}$ is approximated, but without the numerical viscosity. It should be emphasized that central approximation of derivative with the explicit Euler is usually avoided as it can lead to an unstable method. However, the large numerical viscosity of Lax–Friedrichs is a stabilizing factor, and in our case we have had few problems with stability.

HLLC: In deriving the HLLC–method we assumed only to have conservative flux $\mathbf{F}(\mathbf{U})$. To treat $\boldsymbol{\sigma}$ fully would require us to rethink the whole method. However, using the discontinuity wave interpretation of the HLLC–method we can easily generalize it to contain the first term

$$\partial_t \alpha_1 + \mathbf{u} \cdot \boldsymbol{\nabla} \alpha_1 = 0, \tag{5.8}$$

which is simply convection of volume fraction. We could very well add a fourth wave to our method only containing α_1 traveling with speed $\mathbf{u}$. However this is unnecessary as middle velocity wave will move at a speed very close to $\mathbf{u}$, thus we can just add α_1 to our discontinuity wave. The $\Sigma(\mathbf{U}, \boldsymbol{\nabla}\mathbf{U})$ is harder to incorporate and would require more discontinuity waves. In this report we choose the simplest way of dealing with this term, which is to ignore it. This is also what was done in [6], where it was emphasized that simulation of with generalized HLLC including this term differ little from the one without. We would like to stress that we have implemented two different solvers incorporating this term, thus we are not totally dependent on this approximation. Another "flaw" to our approach is the the HLLC–method we use (which was found in [6]) assumes equilibrium of the pressures, thus only allowing for instantaneous relaxation and the ASY-method thus cannot be used.

Roe-scheme: We cannot write our homogeneous system in conservative form. However we can write it in quasilinear form

$$\mathbf{U}_t + \mathbf{A}(\mathbf{U})\mathbf{U}_x = 0, \tag{5.9}$$

opening for a linearized Riemann–solver like that of Roe. Like Roe we seek a matrix $\tilde{\mathbf{A}}$ which satisfies property A and B, that is it has to be hyperbolic and to be consistent with the original $\mathbf{A}$. However, since our system is not conservative we need to modify property C. We replace this property by property[6] $\tilde{\text{C}}$:

- $\tilde{\mathbf{A}}$ should conserve partial densities $\alpha_k \rho_k$, mixture momentum $\rho\mathbf{u}$ and mixture energy E.

With such a matrix we are able to describe fully the homogeneous terms without ignoring anything. For the actual Roe–matrix we refer to [6]. Note that it is only the derivation of the Roe–matrix that changes; when this matrix is obtained we solve the problem just as indicated in section 3.2.3.

With these changes and the methods presented earlier we have all what's needed to treat the homogeneous part.

[6] Mixture energy: $E \equiv= \alpha_1 E_1 + \alpha_2 E_2$

5.3 Relaxation terms

To use the ASY-method, or instantaneous relaxation we need to compute $\mathbf{U}^{eq}$. The problem is the following: Given state $\mathbf{U}^*$, what is the equilibrated state $\mathbf{U}^{eq}$. The relaxation step involves the following set of equations

$$\partial_t \alpha_1 = \mu \left(p_1 - p_2\right) \tag{5.10a}$$
$$\partial_t (\alpha_1 \rho_1) = 0 \tag{5.10b}$$
$$\partial_t (\alpha_2 \rho_2) = 0 \tag{5.10c}$$
$$\partial_t (\rho \mathbf{u}) = 0 \tag{5.10d}$$
$$\partial_t \left(\alpha_1 E_1\right) = -\mu p_I (p_1 - p_2) \tag{5.10e}$$
$$\partial_t \left(\alpha_2 E_2\right) = \mu p_I (p_1 - p_2) \tag{5.10f}$$

First we note that relaxation only involves α and the two different energies. Thus component $n = \{2, 3, 4\}$ of $\mathbf{U}^*$ are unchanged and are the equilibrium values. The three other variables however can change, but not entirely freely. Adding (5.1e) to (5.1f) we get

$$E_t + \boldsymbol{\nabla} \left(E\mathbf{u} + \alpha_1 p_1 \mathbf{u} + \alpha_2 p_2 \mathbf{u}\right) = 0 \tag{5.11}$$

where

$$E \equiv \alpha_1 E_1 + \alpha_2 E_2, \tag{5.12}$$

the mixture energy is conserved. This adds a constraint a to what $\mathbf{U}^{eq}$ might be. However this constraint is not enough for determining uniquely the equilibrium configuration. This becomes clear by writing the two last equations as

$$\partial_t \left(\alpha_1 E_1\right) = -p_I \partial_t \alpha, \tag{5.13a}$$
$$\partial_t \left(\alpha_2 E_2\right) = p_I \partial_t \alpha, \tag{5.13b}$$

which cannot be integrated analytically as p_I, the interface pressure, will change in time. How to overcome this hurdle is one of the biggest innovation presented in [6]. In this paper it was assumed that

$$p_I = p_I^* + \frac{p_I^{eq} - p_I^*}{\alpha_1^{eq} - \alpha_1^*} \left(\alpha_1 - \alpha_1^*\right), \tag{5.14}$$

also shown in figure 5.1. With this approximation we can easily integrate (5.13), and we find that

$$\left(\alpha_1 E_1\right)^{eq} - \left(\alpha_1 E_1\right)^* = -\frac{p_I^* + p_I^{eq}}{2} \left(\alpha_1^{eq} - \alpha_1^*\right) \tag{5.15}$$
$$\left(\alpha_2 E_2\right)^{eq} - \left(\alpha_2 E_2\right)^* = \frac{p_I^* + p_I^{eq}}{2} \left(\alpha_1^{eq} - \alpha_1^*\right) \tag{5.16}$$

giving the connection needed for computing the an approximate equilibrium configuration. We do not intend going through the whole derivation for finding $\mathbf{U}^{eq}$ as it is thoroughly presented in [6]. What we would like however, is to emphasize that this value can be obtained analytically, thus making an approximate value of $\mathbf{U}^{eq}$ available for use in the ASY–method, thus avoiding implicit methods. This gives the final piece needed for implementing numerical simulation of the model system.

5.4 Numerical Implementation and Numerical experiments

A MATLAB program was written[7] to simulate the model system. This program uses a fractional step approach, treating the hyperbolic part separate from the relaxation. The hyperbolic part is solved numerically using Lax–Friedrichs, HLLC and the Roe–scheme. The relaxation part is implemented both with the ASY–method (with small alternation) and by instantaneous equilibrium. Our first focus goes towards replicating the results in [6]. In order to be consistent with the instantaneous relaxation of Pelanti we used the ASY–method however with very fast relaxation, $\mu \sim 1 \times 10^6$.

[7] We could have used a more efficient programming language like FORTRAN or C++. However, we decided that the numerical efficiency gained would not pay for the additional time required for the implementation and debugging. If the simulations were to be generalized to two dimensions, efficiency would have become more important and implementation should be done in a more efficient language.

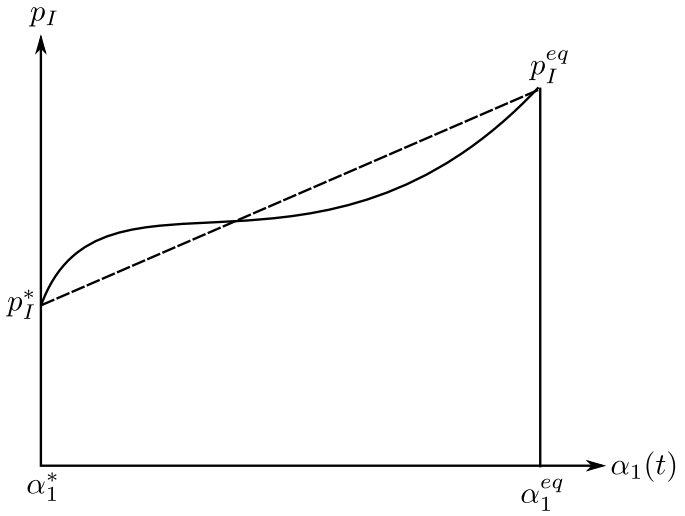

Figure 5.1: Approximation of p_I by a linear extrapolation.

5.4.1 Dodecane Shock Tube

The first numerical experiment we will consider is the liquid–vapor shock tube. A tube of unit length is filled with Dodecane and has an initial discontinuity located at $x = 0.75$. The conditions on the left side are

$$(\rho_v, \rho_l, u, p, \alpha_v) = \left(2\,\mathrm{kg/m^3}, 500\,\mathrm{kg/m^3}, 0, 1 \times 10^8\,\mathrm{Pa}, 10^{-8}\right) \tag{5.17}$$

while on the right side (right of $x > 0.75\,\mathrm{m}$))

$$(\rho_v, \rho_l, u, p, \alpha_v) = \left(2\,\mathrm{kg/m^3}, 500\,\mathrm{kg/m^3}, 0, 1 \times 10^5\,\mathrm{Pa}, 1 - 10^{-8}\right). \tag{5.18}$$

The parameters for the equation of state are given in Table 1. Figure 5.2 shows the results of the

Table 1: Parameters for the stiffened gas equation of state for Dodecane.

Phase	γ	π[Pa]	e^*[J/kg]	C_v[J/kg]
Liquid	2.35	4×10^8	-775.269×10^3	1077.7
Vapor	1.025	0	-237.547×10^3	1956.45

numerical experiment with the parameters above after $t = 473\,\mu\mathrm{s}$ for the HLLC and Lax–Friedrichs method[8] using 10000 cells and CFL–number 0.9. we first look at the overall picture this experiment gives. The experiment starts out uniformly distributed and at equilibrium on each side. Then right after the experiment is started the two fluids start moving due to the pressure difference. This motion is reflected in the plateau we see for the velocity expanding to the left by a rarefaction wave and to the right by a shock. Note that the experiment is short enough so that information cannot reach the left $x = 0\,\mathrm{m}$. Thus the configuration at the far left is unchanged. It is interesting to note how well this experiment is captured in terms of shocks and rarefaction waves.

The results we see are in agreement with those observed in [6] with the exception of the temperature difference which has a twice as high plateau in this paper. We were initially puzzled by this, but became more and more confident that our results were indeed the correct ones. First of all, we are doing the simulation with both Lax–Friedrichs and HLLC. These are two very different methods, yet they give the same plateau. Thus a systematic error is largely out of the question. Combine this with the fact that information travels at finite speed and the time of the experiment is not long enough for information

[8] We tried using the Roe–solver, but it turned to be unstable for this problem. Although Roe is very accurate, it is not as robust as Lax–Friedrichs or HLLC. The problem originates from us almost having an one phase flow at the two sides and Roe is notorious for not being able to handle that. This was also the case in [6] and even in [2] which was on the two fluid model – another model.

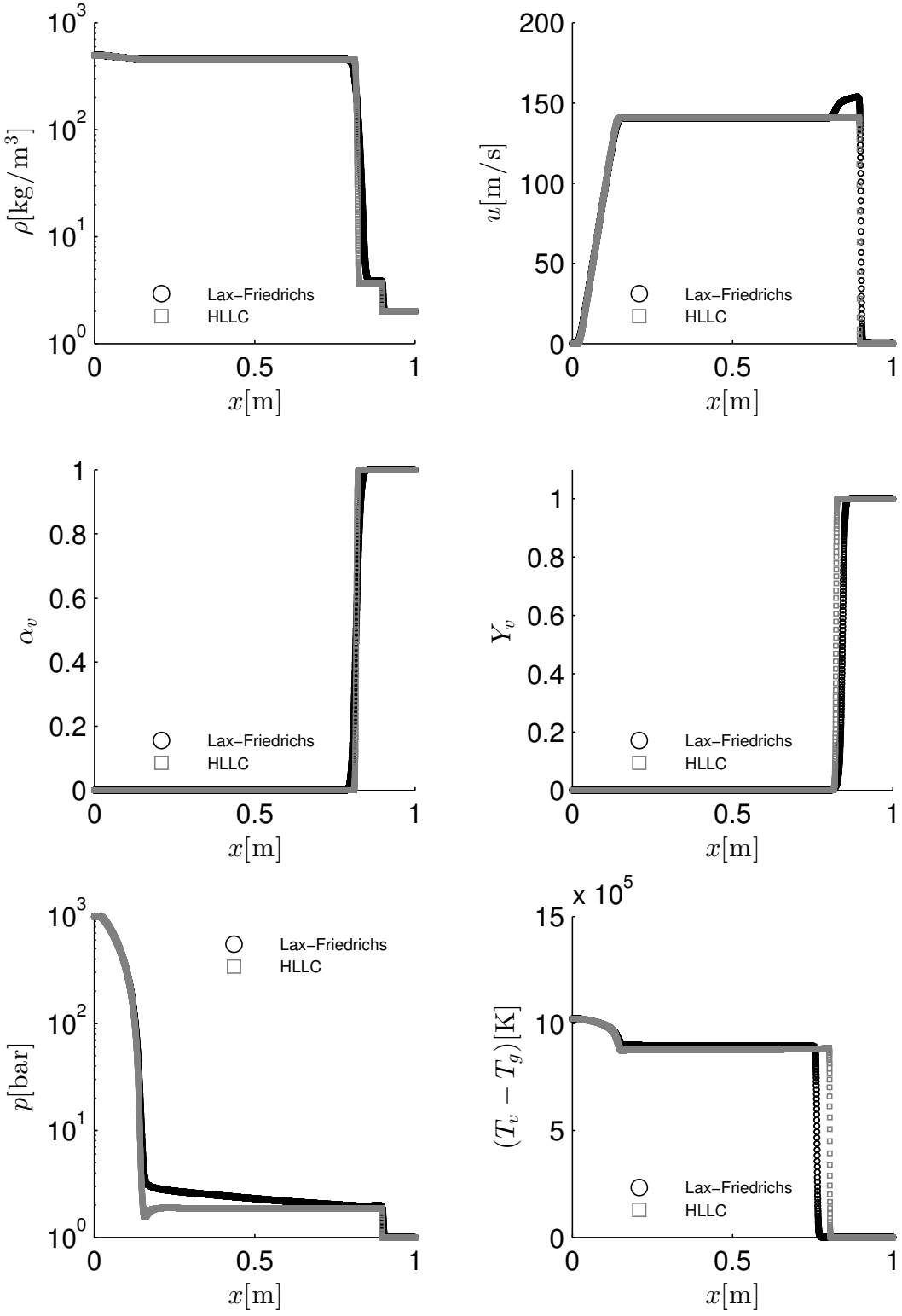

Figure 5.2: Shock tube simulation for Dodecane using the HLLC and Lax–Friedrichs method with 10000 cells and CFL number 0.9.

to travel from $x = 0.75\,\mathrm{m}$ to the left side, leaving the only possibility of wrong initial conditions. We checked our initial conditions and they were consistent with the values given above. Finally all the other graphs agreed. We contacted one of the authors of the paper, Marica Pelanti and she confirmed our results with revised graph with the same plateau as us, see Appendix A.5.

It is interesting to compare the results obtained by the two methods. First we note that the overall behavior is very similar. As expected the HLLC method gives sharper solutions than the Lax–Friedrichs method. The large numerical viscosity of Lax–Friedrichs tends to smear the solutions out. However, this is not the only significant difference between the two. The discontinuities to the left are also positioned differently, and the pressure plateau is different for the two. The are many possible causes for this discrepancy. One plausible candidate is the smearing in Lax–Friedrichs. We initially did the simulation using 5000 cells, increasing to 10000 these discrepancies became smaller, especially the difference of the pressure plateau. Yet there are still differences, like the bump on the top of the velocity graph and difference in position of the temperature discontinuity. A good candidate for such differences are entropy mistakes – the Riemann solver has converged to the wrong weak solution. This is very common for approximate Riemann solvers. Lax–Friedrichs has a large numerical viscosity and will in general have an easier time than the HLLC–solver to choose the right weak solution. Thus it can very well be the that Lax–Friedrichs solution that corresponds more closely to "true" solution than the HLLC. Lastly we should remember that in constructing the HLLC–solver that we ignored the $\mathbf{\Sigma}$-terms. Even if their contribution tends to be small, it could very well cause the small differences we observe. That being said it is very important to emphasize that the Lax–Friedrichs method required many points to give a reasonable solution, while the HLLC could give reasonable results only using 100 points. Normally we will not have the luxury of using lots of points and the Lax–Friedrichs is left useless due to its smearing.

5.4.2 Water cavitation experiment

We are all familiar with the process of boiling, in which a liquid is transformed into gas as the temperature reaches the boiling point. Perhaps less known is that a liquid may undergo the same transformation under a pressure decrease. This process is called cavitation and can be observed in everything from shaken soda bottles to rotating boat propellers. Here we perform a model experiment called cavitation tube. In this experiment a tube is filled with liquid water of density $\rho_l = 1150\,\mathrm{kg/m^3}$ at atmospheric pressure $p = 1 \times 10^5\,\mathrm{Pa}$. The liquid is uniformly distributed with a small amount of vapor $\alpha_v = 1 \times 10^{-2}$. The temperature is $T = 354.728\,\mathrm{K}$ and vapor density of $\rho_v = 0.63\,\mathrm{kg/m^3}$. The origin of the cavitation is a discontinuity in velocity with $u = -2\,\mathrm{m/s}$ on the left and $u = 2\,\mathrm{m/s}$ on the right of the middle. The parameters of the stiffened gas EOS are given in Table 2

Table 2: Parameters for the stiffened gas equation of state for water.

Phase	γ	π[Pa]	e^*[J/kg]	C_v[J/kg]
Liquid	2.35	1×10^9	-1167×10^3	0
Vapor	1.025	0	2030×10^3	-23.4×10^3

In figure 5.3 we see the results after a time $t = 3.2\,\mathrm{ms}$ using HLLC- and the Roe-method. We first consider the overall behavior of the system. As the fluid moves away from the middle a pressure vacuum is left behind. This pressure vacuum causes water to turn into vapor, shown in the peak of volume fraction of α_v. The velocity profile is a rarefaction wave going to the left and right.

The two methods match perfectly each other and are in good agreement with the graphs presented in [6]. There is one discrepancy between our results and those of Pelanti & Shyue. The volume fraction peak is twice as high and sharper than that of Pelanti and Shue. This is most likely due to the fact that we use 10000 points and they use 5000. Thus we are able to capture the sharper peak better than them.

We now do the same numerical experiment, only now we turn up the velocity to $u = 500\,\mathrm{m/s}$. Figure 5.4 shows the results of this. The behavior of the system is similar to that of the previous numerical experiment, but much more violent. Instead of having a small peak in the middle of the tube with vapour, we have a large of portion of water turning entirely into vapour. Again our results match very well with those obtained by Pelanti & Shyue and the two solvers give almost identical solutions.

The performance of the two solvers is very comparable, this despite the Roe–solver being more sophisticated. However due to the eigenstructure of the model this is also to be expected. We only have three distinct eigenvalues for this model – three velocities for which the discontinuity can separate into four different levels. This is also the same number of velocities in the HLLC. Roe allows for six velocities, but only three of them are actually needed. Thus they're both able to capture all the intermediate levels of the model system.

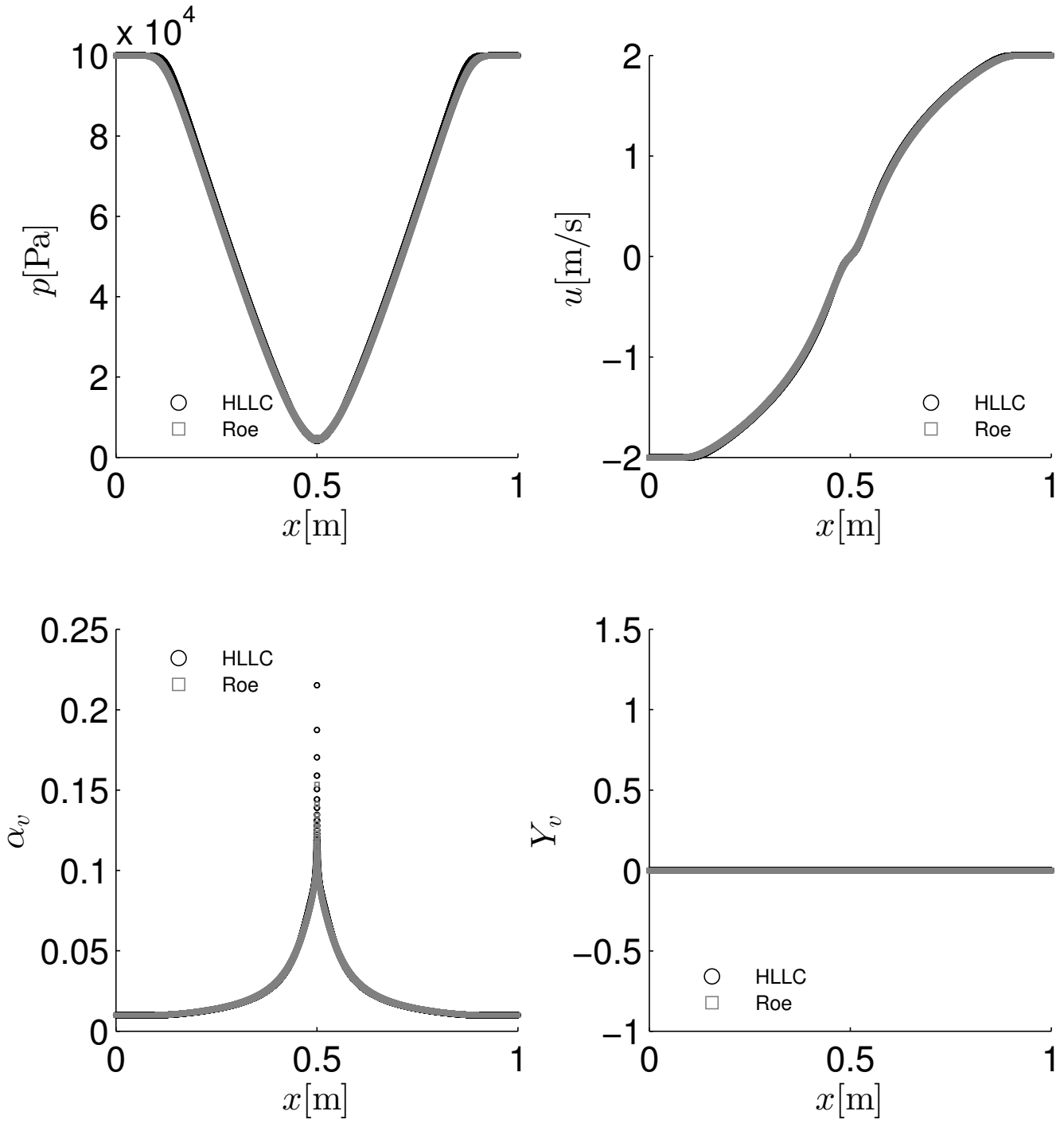

Figure 5.3: Results from cavitation tube experiment with water at $t = 3.2\,\mathrm{ms}$ for $v = 2\,\mathrm{m/s}$ using the HLLC– and Roe–methods. Simulations were done with 10000 cells and a CFL–number of 0.5.

It is interesting to note that for the Cavitation tube our simulations also replicate what is very likely a flaw in the findings of Pelanti & Shyue. A close look at the velocity graph in figure 5.3 reveals a small bump in the middle. This is most likely not a part of the true solution, but an artifact of the approximate Riemann solver we use – an entropy mistake. In fact the initial condition is a textbook example of where transonic rarefaction is the correct solution of the Riemann problem – a rarefaction wave spanning from the left to the right of the cell edge in between the discontinuity. HLLC and Roe will treat this as a shock and thus give a wrong solution.

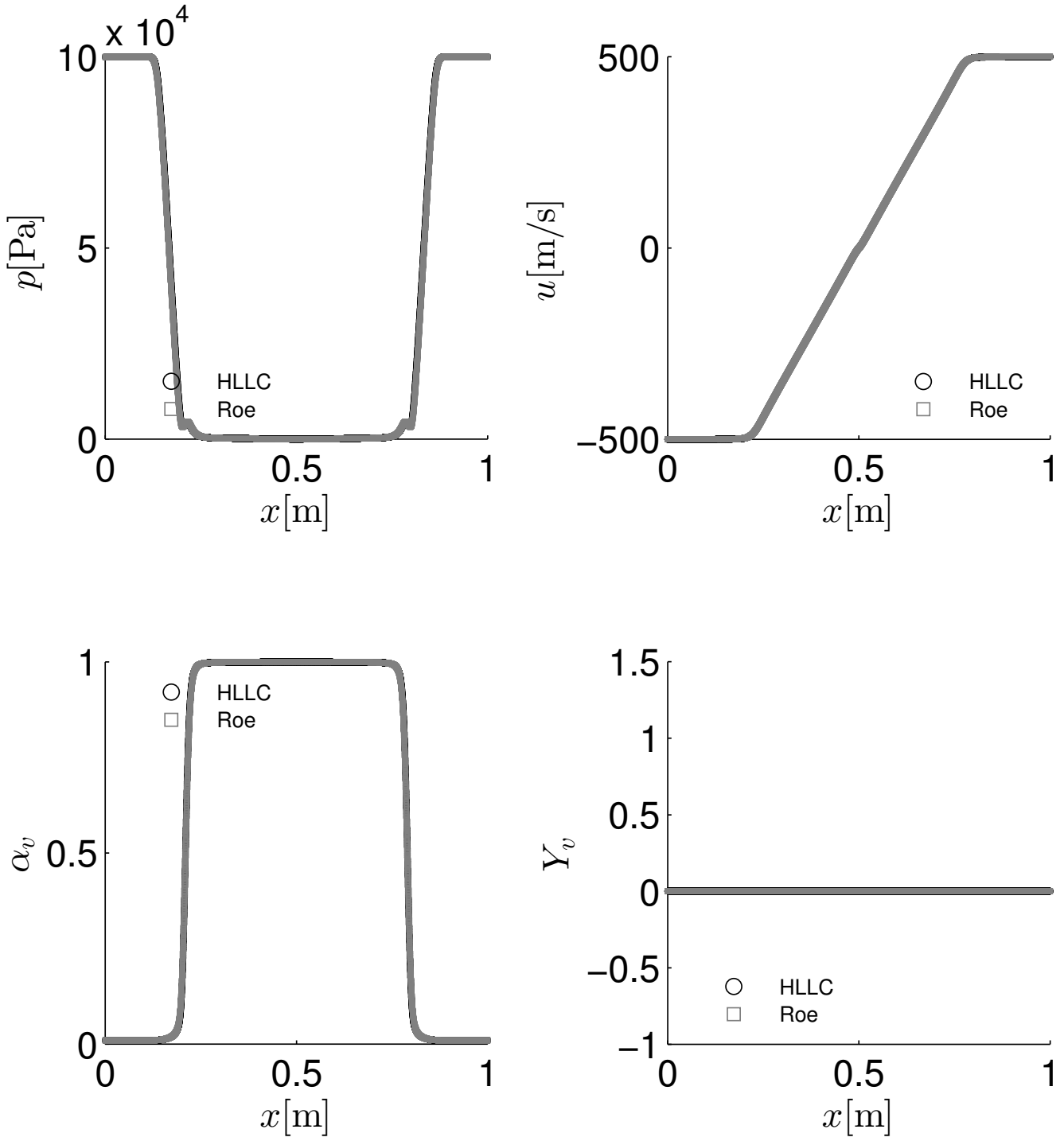

Figure 5.4: Results from cavitation tube experiment with water at $t = 0.58\,\mathrm{ms}$ for $v = 500\,\mathrm{m/s}$ using the HLLC– and Roe–methods. Simulations were done with 10000 cells and a CFL–number of 0.1.

5.4.3 Reflections on the ASY–method

The numerical tests we did also allowed us to test out the ASY–method. Once the equilibrium state is obtained, the ASY–method is very simple to implement. However we quickly met problems with stability. After ruling out simple mistakes in the implementation and ruling out divergences for $U^* = u^{eq}$ we discovered a root of the problem. Ever so often the τ in the ASY–method would be negative. When it is negative, the solution will rather than approach equilibrium, go the opposite way and very much so. For fast relaxation this led to the exponential blowing up and the program to crash. We cannot

be entirely sure that it is not caused by incorrect implementation. However we have some theories as to why we experience this problem. For the ASY–method to work properly, the equilibrium has to be monotonously reached. In figure 5.5 we see line I moronically converging to the correct equilibrium while line II takes a detour before converging to U^{eq}. Such a detour will be reflected in a negative τ and can cause the exponential to diverge for fast relaxation and thus the simulation to crash. However is such a detour possible for the system of equations? We haven't been able to answer this question yet, but just because we seem to experience this in our simulations doesn't mean that it is. Another plausible cause might be the approximation we perform to compute the equilibrium value $\mathbf{U}^{eq}$. This is an approximate value. If it differs from the real equilibrium value we may have situations as shown in figure 5.5 (Right). Here we will have negative τ and possible blowing up of the exponential.

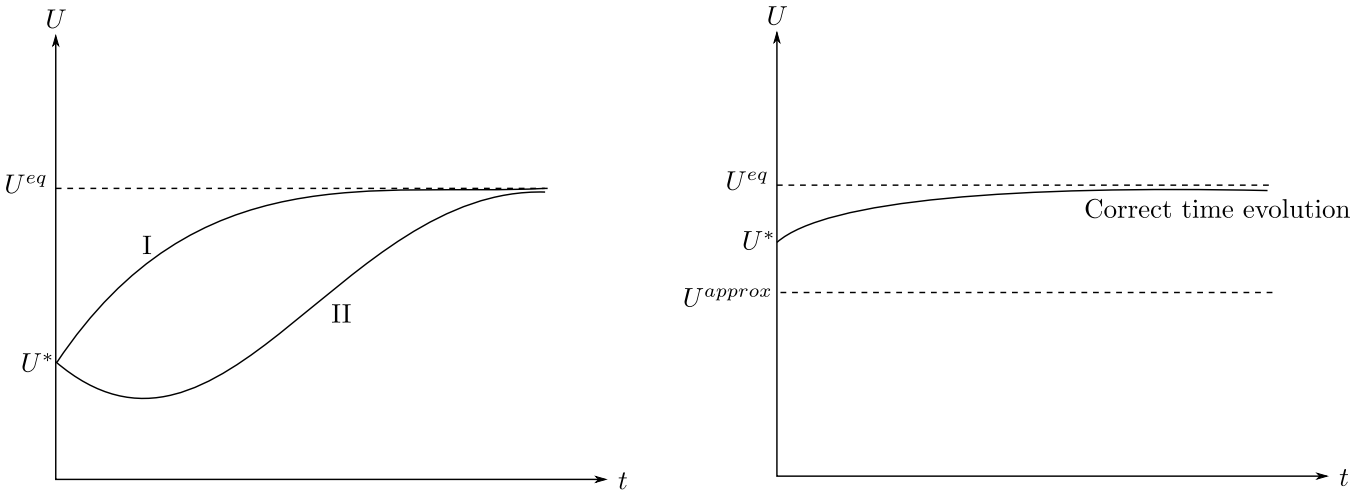

Figure 5.5: (Left) Paths from U^* to U^{eq}. Path I is monotonnically approaching U^{eq}, while II is taking a detour eventually reaching U^{eq}. (Right) Illustration of a situation where the possible approximate value is on the wrong side of U^*, leading to negative τ.

To overcome this problem we chose to tweak the ASY-method by taking the absolute value of τ. By doing so we guarantee that we always go toward the approximate equilibrium value. One can argue that it is only in rare cases that we have negative τ. However one will always in this way bias the problem toward the approximate equilibrium value. This will therefore to some degree also bias how well an ASY–method can be used to model the physics in a problem for which relaxation is slow.

6 Conclusion and future prospects

In this report, we have investigated the six-equation two-phase single velocity model with finite relaxation. This was done using the framework of hyperbolic relaxation systems. Through a thorough introduction, we have presented the theory needed to understand key features of hyperbolic relaxation systems and the methods needed to solve them numerically. Applying these methods we have successfully implemented simulation for the model with finite relaxation.

Using our simulation we were able to replicate and find flaws in the findings of Pelanti & Shyue, presented in [6]. As these simulations were done with three different Riemann solvers, we were also able to compare their suitability for this specific model system. Of the three solvers HLLC preformed the best, having similar accuracy compared to the Roe–solver, but better robustness.

Our simulations also allowed us to investigate the ASY-method – a method which is new and has yet to be tested extensively. Straightforward implementation of the ASY-method turned out to be unstable. There are several possible causes. As always human error in the implementation is a possible source. However, perhaps more likely is that the model breaks the monotonicity requirement of the ASY-method or that the use of an approximate equilibrium value lead to an unstable method. This goes to show that even though the ASY–method has many desirable properties, one should be very careful in applying it beyond its domain of validity. A possible workaround is to tweak the method to always approach equilibrium. By doing so we regain stability. However in doing so we also lose consistency and bias our simulation towards the approximate equilibrium configuration, which might give an unwanted bias to the physics of relaxation.

There many possible avenues to build upon this report. A very natural extension would be to do the simulation in two dimensions. This would allow us to perform advance numerical experiments and to explore cavitation more in detail. Towards the same goal is incorporating other types of relaxations like thermal relaxation and thermochemical relaxation like done in [6]. By doing so we will be able to obtain more realistic results. Also interesting would be to implement relaxation by an implicit method, by doing so we would be able to compare it the ASY-method. This would allow us to determine to what degree the ASY-method with tweak, biases relaxation and whether the monotonicity toward equilibrium is broken in this model.

References

[1] Peder Aursand, Steinar Evje, Tore Flåtten, Knut Erik Teigen Giljarhus, and Svend Tollak Munkejord. An exponential time-differencing method for monotonic relaxation systems. *Applied Numerical Mathematics*, 80(0):1 – 21, 2014.

[2] Steinar Evje and Tore Flåtten. Hybrid flux-splitting schemes for a common two-fluid model. *Journal of Computational Physics*, 192(1):175 – 210, 2003.

[3] T. Flåtten, A. Morin, and S. Munkejord. On solutions to equilibrium problems for systems of stiffened gases. *SIAM Journal on Applied Mathematics*, 71(1):41–67, 2011.

[4] S. K. Godunov. Difference methods for the numerical calculations of discontinuous solutions of the equations of fluid dynamics. *Mat. Sb.*, 47:271–306, 1959. In Russian, translation in: *US Joint Publ. Res. Service, JPRS*, 7226 (1969).

[5] R.J. LeVeque. *Finite Volume Methods for Hyperbolic Problems*. Cambridge Texts in Applied Mathematics. Cambridge University Press, 2002.

[6] Marica Pelanti and Keh-Ming Shyue. A mixture-energy-consistent six-equation two-phase numerical model for fluids with interfaces, cavitation and evaporation waves. *Journal of Computational Physics*, 259(0):331 – 357, 2014.

[7] P. L. Roe. Approximate riemann solvers, parameter vectors and difference schemes. *J. Comput. Phys.*, 43:357–372, 1981.

[8] RICHARD SAUREL, FABIEN PETITPAS, and REMI ABGRALL. Modelling phase transition in metastable liquids: application to cavitating and flashing flows. *Journal of Fluid Mechanics*, 607:313–350, 7 2008.

[9] E.F. Toro, M. Spruce, and W. Speares. Restoration of the contact surface in the hll-riemann solver. *Shock Waves*, 4(1):25–34, 1994.

A Appendix

A.1 Closing the system and Macroscopical variables

The varibles in (1.3), that is

$$\mathbf{U} = \begin{pmatrix} \alpha_1 \\ \alpha_1\rho_1 \\ \alpha_2\rho_2 \\ \rho\mathbf{u} \\ \alpha_1 E_1 \\ \alpha_2 E_2 \end{pmatrix}, \tag{A.1}$$

are by no means unique. However they have desirable properties in that the momentum of each phase, and the total energy $E = \alpha_1 E_1 + \alpha_2 E_2$ is conserved. Using these variables one can design numerical schemes which guarantees these conservations. However, these microscopical variables are not typically the variables of interest when evaluating the data. Typically what one is interested in are the macrocopical variables likes temperature and pressure. Using the equation of state one could also derive the set of equations for

$$\mathbf{V} = \begin{pmatrix} \alpha_1 \\ \mathbf{u} \\ T_1 \\ T_2 \\ P_1 \\ P_2 \end{pmatrix}, \tag{A.2}$$

which represents variables that are easy to measure in an experiment and give more macroscopic picture. Keeping in mind we want a conservative scheme and that the variables of interest in the end are the macroscopical variables of (A.2), we are interested in finding a transformation between between (A.1) and (A.2). Not only is such a transformation useful in the end to transform microscopical data into macroscopical data, it is also useful as such transformation provides the information needed to close system of equations. Using the stiffened gas EOS we derive the following transformation from (A.1) to A.2 (assuming one dimension)

$$\mathbf{V} = G(\mathbf{U}) = \begin{pmatrix} U_1 \\ \frac{U_4}{U_2+U_3} \\ \frac{1}{C_v}\left(\frac{U_5}{U_2} - \frac{1}{2}V_2^2 - e_1^* - \frac{U_1\pi_1}{U_2}\right) \\ \frac{1}{C_v}\left(\frac{U_6}{U_3} - \frac{1}{2}V_2^2 - e_2^* - \frac{(1-U_1)\pi_2}{U_3}\right) \\ (\gamma_1 - 1)\frac{U_2}{U_1}\left(\frac{U_5}{U_2} - \frac{1}{2}V_2^2 - e_1^*\right) - \gamma_1\pi_1 \\ (\gamma_2 - 1)\frac{U_3}{1-U_1}\left(\frac{U_6}{U_3} - \frac{1}{2}V_2^2 - e_2^*\right) - \gamma_2\pi_2 \end{pmatrix}. \tag{A.3}$$

For completeness we also provide the inverse operation which is useful as check and in obtaining initial conditions from data given in macroscopic variables

$$\mathbf{U} = G^{-1}(\mathbf{V}) = \begin{pmatrix} V_1 \\ V_1\frac{V_5+\pi_1}{C_{v1}V_3(\gamma_1-1)} \\ (1-V_1)\frac{V_6+\pi_2}{C_{v2}V_4(\gamma_2-1)} \\ V_2(U_2+U_3) \\ U_2(C_{v1}V_3\frac{V_5+\gamma_1\pi_1}{V_5+\pi_1} + e_1^* + \frac{1}{2}V_2^2) \\ U_2(C_{v2}V_4\frac{V_6+\gamma_2\pi_2}{V_6+\pi_2} + e_2^* + \frac{1}{2}V_2^2) \end{pmatrix} \tag{A.4}$$

A.2 Eigenstructure

The homogeneous part can be diagonalized. The eigenvalues are given by

$$\lambda_1 = u - c, \quad \lambda_2 = \lambda_3 = \lambda_4 = \lambda_5 = u, \quad \lambda_6 = u + c. \tag{A.5}$$

with eigenvectors

$$\mathbf{R}(\mathbf{U}) = \begin{pmatrix} 0 & 0 & 0 & 0 & 1 & 0 \\ Y_1 & 0 & 0 & 1 & 0 & Y_1 \\ Y_2 & 0 & 1 & 0 & 0 & Y_2 \\ u-c & 0 & u & u & 0 & u+c \\ Y_1(H_1-uc) & -\frac{\kappa_2}{\kappa_1} & \frac{\kappa_2}{\kappa_1}H_2 - \frac{c_2^2}{\kappa_1} & H_1 - \frac{c_1^2}{\kappa_1} & \frac{\Pi_1-\Pi_2}{\kappa_1} & Y_1\left(H_1+uc\right) \\ Y_1(H_2-uc) & 1 & 0 & 0 & 0 & Y_2\left(H_2+uc\right) \end{pmatrix}, \tag{A.6}$$

where H_k is the total enthalpy, $\Pi_k = -\rho_k c_k^2 + p_k(1+\kappa_k)$, with $\kappa_k = \frac{\partial p_k}{\partial \mathcal{E}_k}$

A.3 Transformation

$$E_k = \rho_k \left(e_k + \frac{1}{2}\mathbf{u}^2\right) \tag{A.7}$$

$$e_k - e_k^* = C_v T_k + \frac{\pi_k}{\rho_k} \tag{A.8}$$

$$T_k = \frac{1}{C_v}\left(e_k - e_k^* - \frac{\pi_k}{\rho_k}\right) \tag{A.9}$$

$$T_k = \frac{1}{C_v}\left(\frac{E_k}{\rho_k} - \frac{1}{2}\mathbf{u}^2 - e_k^* - \frac{\pi_k}{\rho_k}\right) \tag{A.10}$$

$$T_k = \frac{1}{C_v}\left(\frac{\alpha_k E_k}{\alpha_k \rho_k} - \frac{1}{2}\mathbf{u}^2 - e_k^* - \frac{\pi_k}{\rho_k}\right) \tag{A.11}$$

In terms $\mathbf{U}$ for

$$T_1 = \frac{1}{C_v}\left(\frac{U_5}{U_2} - \frac{1}{2}V_2^2 - e_1^* - \frac{U_1\pi_1}{U_2}\right) \tag{A.12}$$

$$T_2 = \frac{1}{C_v}\left(\frac{U_6}{U_3} - \frac{1}{2}V_2^2 - e_2^* - \frac{(1-U_1)\pi_2}{U_3}\right) \tag{A.13}$$

Pressure

$$p_k = (\gamma_k - 1)\rho_k\left(e_k - e_k^*\right) - \gamma_k \pi_k \tag{A.14}$$

$$p_k = (\gamma_k - 1)\rho_k\left(\frac{\alpha_k E_k}{\alpha_k \rho_k} - \frac{1}{2}\mathbf{u}^2 - e_k^*\right) - \gamma_k \pi_k \tag{A.15}$$

In terms of $\mathbf{U}$

$$p_1 = (\gamma_1 - 1)\frac{U_2}{U_1}\left(\frac{U_5}{U_2} - \frac{1}{2}\mathbf{V}_2^2 - e_1^*\right) - \gamma_1\pi_1 \tag{A.16}$$

$$p_1 = (\gamma_2 - 1)\frac{U_3}{1-U_1}\left(\frac{U_6}{U_3} - \frac{1}{2}\mathbf{V}_2^2 - e_2^*\right) - \gamma_2\pi_2 \tag{A.17}$$

A.4 From V to U

$$e_k - e_k^* = C_{Vk} T_k \frac{p_k + \gamma_k \pi_k}{p_k + \pi_k} \tag{A.18}$$

$$\rho_k = \frac{p_k + \gamma_k \pi_k}{C_{vk} T_k (\gamma_k - 1)} \frac{p_k + \pi_k}{p_k + \gamma_k \pi_k} \tag{A.19}$$

$$\rho_k = \frac{p_k + \pi_k}{C_{vk} T_k (\gamma_k - 1)} \tag{A.20}$$

$$U_2 = V_1 \frac{V_5 + \pi_1}{C_{v1} V_3 (\gamma_1 - 1)} \tag{A.21}$$

$$U_3 = (1 - V_1)\frac{V_6 + \pi_2}{C_{v2} V_4 (\gamma_2 - 1)} \tag{A.22}$$

A.5 Revised Temperature Difference Graph

After discussion with the author of [6] she sent us the revised graph shown in figure A.1

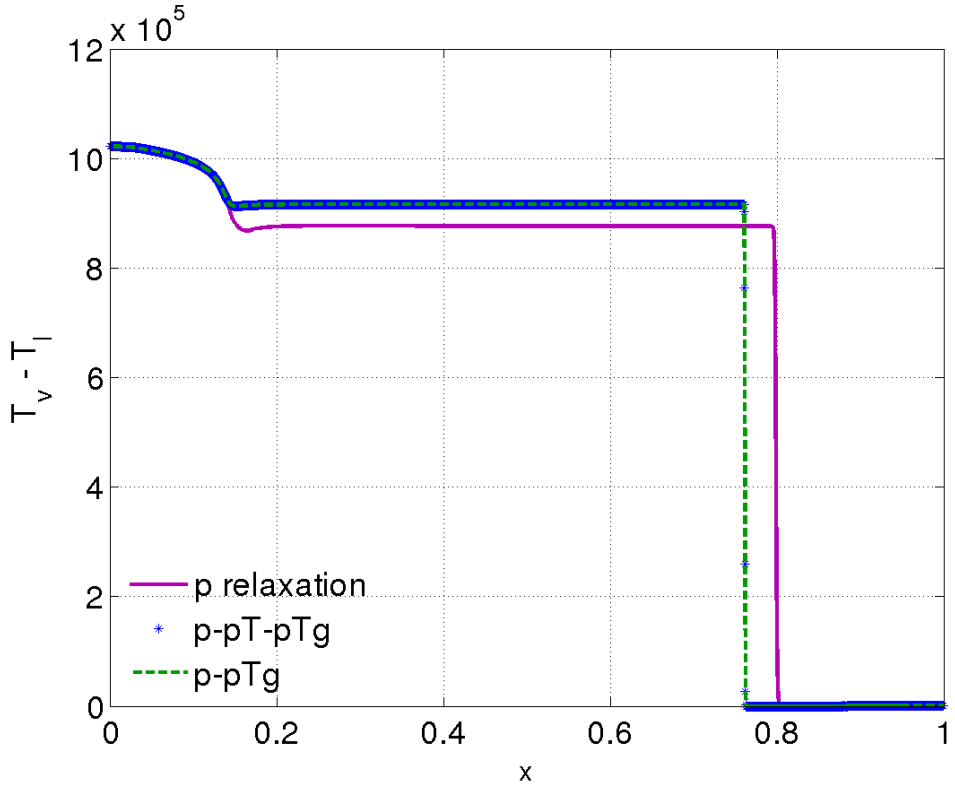

Figure A.1: Revised graph of temperature difference by Marica Pelanti. Note that p–relaxation is only important to us, the others correspond to different relaxation.